Sex differences in the role of parabrachial in nociception and pain in awake mice

Abbreviated title: Parabrachial in nociception and pain in awake mice

Jesse Smith[1], Yadong Ji[2], Rebecca Lorsung[1], Macauley Breault[3], Jeffrey Koenig[4], Nathan Cramer[1], Radi Masri[1,2], Asaf Keller[1]

[1] University of Maryland, Program in Neuroscience, Department of Anatomy and Neurobiology
[2] Department of Advanced Oral Sciences and Therapeutics, University of Maryland School of Dentistry
[3] Picower Institute for Learning and Memory, Massachusetts Institute of Technology, Cambridge, MA, USA
[4] University of Maryland, Program in Molecular Medicine, Department of Anatomy and Neurobiology

The authors declare no competing financial interests.

Correspondence should be addressed to Asaf Keller at akeller@som.umaryland.edu

63 pages: 63; 10 figures, 1 table
Number of words: Abstract - 198; Introduction - 501; Discussion – 1701

This work was supported by National Institutes of Health National Institute of Neurological Disorders and Stroke Grants R01NS099245 and R01NS069568. The content is solely the responsibility of the authors and does not necessarily represent the official views of the National Institutes of Health. The funding sources had no role in study design; the collection, analysis and interpretation of data; the writing of the report; or in the decision to submit the article for publication. We thank the University of Maryland School of Medicine's Confocal Microscopy Core – Baltimore, Maryland, for supplying the Imaris license.

Abstract

The parabrachial nuclear complex is a nexus for aversion, and for the sensory and affective components of pain perception. We have previously shown that, during chronic pain, parabrachial neurons in anesthetized rodents have amplified activity. We report a method to record from parabrachial neurons of behaving, head-restrained mice, while applying reproducible noxious stimuli. We find that both spontaneous and evoked activity are considerably higher in awake animals. We show that these neurons can be rapidly conditioned to respond to innocuous stimuli, after pairing with nociceptive stimuli. In both males and females with neuropathic or inflammatory pain, responses of parabrachial neurons remain amplified for at least 6 weeks, in parallel with increased pain metrics. Fiber photometry of calcium responses from CGRP-expressing parabrachial neurons in male mice demonstrate that they respond to nociceptive stimuli, and that their responses are amplified in inflammatory pain. In contrast, in females these neurons evoke smaller responses at baseline, and only small increases in neuropathic pain. This sex difference may relate to our finding that, in females, a small percentage of neurons expresses CGRP RNA. Finally, we show that changes in parabrachial activity are correlated with changes in arousal, measured as changes in pupil diameter.

Significance Statement

The parabrachial complex is a nexus of aversion, including pain. We report a method to record from parabrachial neurons of behaving mice, while applying reproducible noxious stimuli. This allowed, for the first time, tracking the activity of these neurons over time in animals with neuropathic or inflammatory pain. It also allowed us to show that the activity of these neurons correlates with arousal states, and that these neurons can be conditioned to respond to innocuous stimuli. Finally, we report substantial sex differences in these neurons.

Introduction

Chronic pain is a major societal and economic problem. Over 20% of Americans are experiencing chronic pain (Zelaya et al., 2020), resulting in profound reductions in quality of life (Smith et al., 2007; O'Connor and Dworkin 2009), and an annual financial burden exceeding $650 billion (Institute of Medicine Committee on Advancing Pain Research, Care, and Education, 2011). Pain is a multidimensional experience, composed of unpleasant sensory, affective and cognitive experiences (Fields, 1999; Melzack and Casey, 1968; Price, 2000; Treede et al., 2000; Auvray et al., 2010). Because of the multidimensionality of the pain experience, chronic pain patients suffer from comorbid emotional disorders and cognitive deficits, and exhibit alterations in the function of brain networks linked to emotional and cognitive deficits (Borsook, 2012; Bushnell et al., 2013). Therefore, treating pain, and especially chronic pain, requires addressing not only the sensory aspects of pain, but also its affective and cognitive components.

Chronic pain affecting the trigeminal system, in particular, is associated with deficits in affective processing, including increases in anxiety and depression (Smith et al., 2013; Wu et al., 2015; de Melo Turnes et al., 2022). A key region in this process is the parabrachial nuclear complex (parabrachial). It is a nexus of aversion, including both the nociceptive and affective components of pain processing (Chiang et al., 2019). Parabrachial is involved in other aversive behaviors (Cai et al., 2018), including taste aversion (Carter et al., 2015, Chen et al., 2018) threat memory (Han et al., 2015), and fear conditioning (Campos et al., 2018; Bowen et al., 2020). We and others have found that parabrachial neurons respond to noxious stimuli under urethane anesthesia (Bernard and Besson, 1990; Uddin et al., 2021) and display amplified activity during chronic pain (Uddin et al., 2018; Raver et al., 2020).

Most of what is known about the physiology of parabrachial in the context of pain comes from studies using anesthetized animals. This is problematic because anesthesia blunts pain related activity and does not allow studies of state-dependent changes in pain perception, which are critical to pain behavior. Pain perception depends on both external stimuli and the internal state of the animal. Internal states—such as distraction (Buhle and Wager, 2010; Legrain et al., 2011) or hunger (Alhadeff et al., 2018)—profoundly alter pain perception. Therefore, it is essential to determine how internal states affect parabrachial processing in behaving animals.

Recordings of nociceptive responses from parabrachial in awake animals are complicated by at least two major technical difficulties. First, the location of parabrachial—at the junction of the midbrain and pons and its relation to major vessels—renders recordings from single units unstable and of low signal to noise ratio in behaving animals. The second complication is the ability to present to behaving animals reproducible noxious stimuli. We have adapted a head-restrained, awake rodent recording model to address these issues. This allowed us to investigate the physiology of parabrachial in awake animals in response to both noxious and non-noxious stimuli and the role of internal states in parabrachial processing.

Methods

We adhered to accepted standards for rigorous study design and reporting to maximize the reproducibility and translational potential of our findings, as described by Landis et al. (2012) and in ARRIVE (Animal Research: Reporting In Vivo Experiments). In line with National Institutes of Health recommendations for scientific rigor, we performed an a priori power analysis to estimate required sample sizes (Landis et al., 2012).

Animals

All procedures were conducted according to Animal Welfare Act regulations and Public Health Service guidelines and approved by the University of Maryland School of Medicine Animal Care and Use Committee. We used 27 male and female wild type C57BL/6 mice from Jackson Laboratory (JAX strain # 000644): 9 CCI-ION animals, 4 CFA injected animals, and 14 naïve animals. We also used 16 CGRP-CRE mice, 8 male and 8 female, that were bred in house from breeding pairs obtained from Jackson Laboratory (JAX stock # 033168).

Animals were housed in a 12 h dark/light cycle, and food and water were given ad libitum. The animals were group-housed prior to headplate surgery. After surgery they were individually housed.

Headplate Implant Surgery

Animals were induced with 2-4% isoflurane and placed in a stereotaxic frame. The anesthesia was maintained at 1-2% for the surgery. Animals were given Rimadyl (5 mg/kg) for analgesia. The skin on the top of the skull was removed and the headplate (Model 11, Neurotar, Helsinki, Finland) was secured to the skull using a mixture of dental cement and Vetbond (3M, USA). Two screws were implanted anterior to the headplate for grounding. A craniotomy was created to expose the brain above parabrachial (AP 4.8mm-5.3mm, ML 0.5mm-2mm) and the dura was removed. The area was cleaned using a cortical buffer with antibiotics (125mM NaCl, 5mM KCl, 10mM Glucose, 10mM HEPES, 2mM 1M $CaCl_2$, 2mM 1M $MgCl_2$, 100 units/ml penicillin, 0.1 mg/ml streptomycin). The craniotomy was closed using a silicone elastomer (QuikSil, World Precision Instruments, Sarasota, FL, USA). The animal was placed on a heating pad and allowed to recover.

Training

Animals were trained on the Neurotar Mobile HomeCage (Neurotar) where they were head restrained, but allowed to locomote freely on a carbon fiber platform supported by a cushion of air. Animals were given 5 days to recover after the implant of the headplate. On day 6 animals were left in their home cage and placed near the Neurotar setup to habituate to the noise of the air flow for 2 hours. On day 7, animals were placed in the Neurotar setup and allowed to move freely for up to 2 hours to habituate to the device. Electrophysiology recordings started on day 8.

Electrophysiology Recordings

Awake Electrophysiology Recordings

We performed recordings in low light conditions. Animals were placed in the Neurotar

setup and allowed to acclimate for 5 minutes. The silicone elastomer was removed and the craniotomy was cleaned using a cortical buffer with antibiotics. A single platinum-iridium recording electrode (0.3-1 MΩ), produced in our lab, was lowered into parabrachial. We digitized recorded waveforms using a Plexon system (Plexon Inc., Dallas, TX). We isolated units that were responsive to noxious heat (50ºC) applied to the anterior maxillary region of the head using a Picasso Lite dental surgical laser (AMD Lasers, Indianapolis, IN), positioned 5 mm above the skin, set to 3.5 W for 5 seconds. The laser was calibrated with a Jenco Electronics microcomputer thermometer to generate 51°C at the end of a 5 s exposure. We waited at least 2 minutes between consecutive stimuli and inspected the skin after each stimulus for erythema or tissue damage. Upon finding a neuron that was responsive to noxious heat stimulation, we allowed the cell to return to its baseline firing rate before recording baseline spontaneous activity for 5 minutes. After that, we recorded responses to noxious heat applied at 2 minute intervals to prevent tissue damage for a total of 10-12 trials. After each recording session, the electrode was removed and the craniotomy was cleaned using a cortical buffer with antibiotics and covered with fresh silicone elastomer.

Anesthetized Electrophysiology Recordings

Animals were anesthetized via intraperitoneal injections of urethane (10% w/v). Following anesthesia, the mice were placed in a stereotaxic frame with a heating pad and a craniotomy was made over the recording site to target parabrachial (AP 4.8mm-5.3mm, ML 0.5mm-2mm). The recording and stimulation protocol was identical to the awake mice protocol.

Electrophysiology Data Analysis

Recordings were sorted using Offline Sorter (Plexon Inc., Dallas, TX) using dual thresholds and principal component analysis. Responses to thermal stimuli were analyzed with custom MATLAB scripts. Significant responses were defined as firing activity exceeding the 95% confidence interval of the average pre-stimulus firing rate. Peristimulus time histograms (PSTHs) were generated to analyze responses to repeated stimuli.

We defined after-discharges—periods of sustained activity that outlast a stimulus presentation (Okubo et al., 2013)—as PSTH bins in which activity exceeded the 95% confidence interval for a period lasting at least 5 seconds after stimulus offset.

CCI-ION

We used a rodent model of neuropathic pain that was induced by chronic constriction of the infraorbital nerve (CCI-ION) (Bennet and Xie, 1988; Uddin et al., 2018; Raver et al., 2020). Animals were anesthetized with ketamine/xylazine (100/10 mg/kg, i.p.). We made intraoral incisions along the roof of the mouth, beginning distal to the first molar. The ION was freed from the surrounding connective tissue and loosely tied with a silk thread (4-0) 1-2 mm from the nerves emerging from the infraorbital foramen. Animals were monitored for 2 days in their home cage as they recovered. Each animal served as its own control, as recordings were compared before and after CCI in each animal.

CFA

We used complete Freund's adjuvant (CFA) to induce persistent inflammatory pain. Animals were induced with 2-4% isoflurane and injected with 15 μL of CFA (Sigma-Aldrich F5881. Sigma, St. Louis, MO, USA) subcutaneously in the snout, ipsilateral to the recording site. Animals were monitored for 24 hours in their home cage as they recovered before recording. Each animal served as its own control, s above.

Behavior

Facial Grimace

To assess ongoing pain, we analyzed facial grimace behaviors in animals placed in the Neurotar Mobile HomeCage and images of the face were taken every 60 seconds for 15 minutes. Animals were scored with defined action units (AU) that examined orbital tightening, nose bulging, whisker positioning, and cheek bulging to derive a mouse grimace score (MGS; Langford et al., 2010; Akintola et al., 2017). We calculated MGS as the average score of all the AUs.

Mechanical Sensitivity

To assess mechanical sensitivity, animals were placed in the Neurotar Mobile HomeCage and von Frey filaments (North Coast Medical) were applied to the anterior maxillary region, ipsilateral to CCI or CFA injections. A response was defined by an active swipe of the filament with the forepaws. We used the up-down method to determine response thresholds, as described previously (Dixon, 1965; Chaplan et al., 1994; Akintola et al., 2017; Raver et al., 2020). For each mouse, baseline response thresholds were determined prior to CCI-ION/CFA injections and thresholds were reassessed on each day of recordings from parabrachial. Hyperalgesia was defined as mechanical withdrawal threshold ≥ 20% below baseline.

Viral Construct Injection

We anesthetized the animals with isoflurane and placed them in a stereotaxic frame. Either left or right parabrachial (-5.2mm AP, ±1.5mm ML, -2.2 to -2.5mm DV) was targeted via a small craniotomy. We injected 0.5 μL of AAV9-syn.Flex.GCaMP6f.WPRE.SV40 (Addgene #100833) at a rate of 0.1 μL/min using glass pipettes (40-60 μm tip diameter), coupled to a Hamilton syringe controlled by a motorized pump. The pipette was left in place for 10 min before being slowly retracted over 5-10 min. Headplates were implanted immediately after the virus injections.

Fiber Photometry

Recording

We anesthetized animals using 2% isoflurane and placed them in a stereotaxic frame. Mice were implanted with a fiber optic probe (400 μM diameter, 0.39NA; RWD Life Sciences) in the parabrachial (-5.2mm AP, +1.5mm ML, -2.2 to -2.5mm DV) during the same surgery they were injected with the viral construct and the head plate was implanted. The mice were given 3 weeks to recover and to allow for viral expression in their home cage.

For recordings, the fiber optic probe was connected to an RZX10 LUX fiber photometry

processor running Synapse software (Tucker-Davis Technologies) through a Doric mini cube (Doric Lenses). LEDs at 465 nm and 405 nm were used for GCaMP excitation and isosbestic control, respectively. LED power was calibrated weekly using a digital optical power meter (Thor Labs).

Analysis

We used pMat (Bruno et al., 2021) to quantify photometry signals as changes in GCaMP fluorescence. These were converted to Z-Scores that were time-locked using a time window starting 5 seconds before the onset of the noxious stimulus and lasting until 30 seconds post-stimulus for each trial. A significant response was defined as one exceeding the 95% confidence interval of the baseline across all trials. The duration and AUC were calculated using the significant response of the Z-Score averaged across trials.

Conditioning

Recordings

Mice were head restrained in the Neurotar Mobile Homecage and recordings were determined to be responsive to noxious heat (see above). While recording pupil size (see below) and firing rate of parabrachial neurons, we presented the mouse with a tone (1 sec, 100 kHz, 88 dB) 10 times with 2 minutes intervals. We administered a conditioning paradigm where a 1 sec tone (CS) was paired with a 5 sec noxious heat stimulus (US), where the tone was presented 3 sec after the onset of the noxious heat, to align with the laser reaching noxious temperature. This pairing was repeated 15 times at 1 minute intervals. The CS was presented until extinction with 2 min between presentations of the CS. We then administered the conditioning paradigm a second time. The CS was again presented until extinction.

The firing rates of conditioned trials were binned at 0.1 seconds before being split into trials time-locked at the stimuli onset. A significant response was defined as exceeding the 95% confidence interval of the baseline across all trials.

Pupillometry

We videotaped pupils in head restrained mice, under low light conditions using a webcam (Logitech Brio, Logitech Inc., Newark, CA). Recordings were acquired at 30 Hz using custom MATLAB® scripts and the Image Acquisition Toolbox (Mathworks, Natick, MA). Noxious heat stimulation timestamps were recorded by a microcontroller (Arduino Uno R3, 2015) using a custom script in Python (Python Software Foundation, https://www.python.org/). These timestamps aligned the video with the electrophysiological data. Pupil area was measured from the videos offline using Facemap software (Stringer et al., 2019). We excluded times when Facemap detected that the animal blinked. Pupil area was normalized using its maximum value within each recording session. Normalized pupil areas of conditioned trials were binned at 0.1 seconds before being split into trials time-locked at the stimuli onset. A significant response was defined as exceeding the 95% confidence interval of the baseline across all trials.

We defined spontaneous activity as activity at least 3 minutes before the onset of the first stimulus. Firing rates and normalized pupil areas during this time were binned using

a width of 1 second. The normalized pupil areas were down-sampled to accommodate the bins of the spike rate by calculating the median within each bin. We applied a minimum cut-off of 10 Hz to the firing rates. To investigate the relationship between spontaneous activity and normalized pupil area we quantified it as the Pearson correlation coefficient.

We then binned firing rates and normalized pupil areas using a width of 0.1 seconds and split them into trials, time-locked around the stimulus onsets. To determine the relative time dynamics between firing rates and normalized pupil area after heat stimuli trials, we calculated a cross-correlation to produce lag values. The lag that maximized the magnitude of correlation was selected for further analysis. The firing rates and normalized pupil area used for cross-correlation were then shifted using this lag before taking the Pearson correlation coefficient.

RNAscope

We collected brains from formalin-perfused, 5-month-old Calca^{Cre} mice (The Jackson Laboratory), sectioned (12 μm thick) and mounted frozen sections cryoprotected with optimal cutting temperature (Sakura) onto Superfrost Plus Slides (Thermo Fisher Scientific). We processed sections in three AP planes for each brain (From 3 male and 3 female mice) for a total of 18 sections, and quantified mRNA transcripts encoding the gene transcript for CGRP (*Calca*) using RNAscope (Advanced Cell Diagnostics, Inc.) with integrated co-detection of NeuN protein. According to manufacturer's instructions, we performed tissue blocking and antigen retrieval prior to an overnight incubation at 4ºC with rabbit anti-NeuN antibody (1:500, ABN78, Millipore Sigma). We then performed RNAscope hybridization using probe Mm-Calca-tv2tv3 - Mus musculus calcitonin/calcitonin-related polypeptide alpha transcript variant 2 (420361) with fluorophore Opal 650 (1:3000, Advanced Cell Diagnostics, Inc.) prior to a 30-minute secondary conjugation with Cy3-conjugated donkey anti-rabbit (1:250, AP182C, Millipore Sigma) and counterstaining/mounting with ProLong Gold Antifade Mountant with DAPI (Invitrogen).

Following RNAscope, we quantified *Calca*+ parabrachial neurons from images photographed with a Leica microsystems TCS SP8 confocoal microscope. Excitation and detection parameters were held constant across all sections. The parabrachial was imaged using a 40x oil immersion objective. Z-stacks were sampled every 3 μm, with each image composed of 7-9 planes. Sections were reconstructed using Leica Las X Navigator tiling software and analyzed using Imaris (Oxford Instruments). Briefly, parabrachial regions of interest (ROI) were selected based on anatomical landmarks described in the 3rd edition of "The Mouse Brain in Stereotaxic Coordinantes" (Paxinos et al., 2020). The size and orientation of these ROIs were held constant across all sections in an AP plane to limit selection bias. Within these defined parabrachial ROIs, Imaris Surfaces was used to select DAPI+ nuclei which were co-labeled with Cy3; these Surfaces were considered neuronal nuclei. The sum of *Calca* channel intensity within each neuronal nucleus was quantified. The lower threshold for *Calca*+ neuronal nuclei was defined for each individual slice by assessing background *Calca* intensity found in a medial pons region with low *Calca* expression ,such as the periaqueductal gray (Allen Brain Atlas, ISH). Neuronal nuclei which fell below this threshold were considered

negative and excluded from further analysis.

Statistical analysis

We analyzed group data using GraphPad Prism version 9 for Mac (GraphPad Software, La Jolla CA) and custom scripts in MATLAB or Python. Data are presented, unless otherwise noted, as median ± 95% confidence intervals (95% CI). We used nonparametric Mann-Whitney *U* tests because data were not normally distributed. Individual statistical tests were run for each animal, as shown in the figures. We then averaged together all animals for each condition and Cohen's *d* was calculated for effect size. All correlations are Spearman's correlations.

Results

Anesthesia suppresses spontaneous and evoked parabrachial responses

Parabrachial neurons recorded in anesthetized animals respond robustly to nociceptive inputs (Bernard and Besson, 1990; Uddin et al., 2018; Raver et al., 2020; Uddin et al., 2021). We developed an approach to apply reproducible noxious stimuli to awake, head-restrained mice, while recording well-isolated single units from the parabrachial nuclear complex (Figs. 1, 2). Nociceptive stimuli were generated by a laser-generated light spot (3mm diameter) applied to the snout. This generated a heat stimulus that increased—during the 5 second stimulus period—from body temperature to 50°C (red bar in Fig. 1). Figure 1 compares examples of peri-event histograms recorded from individual parabrachial neurons in an anesthetized mouse (Fig. 1A) and in an awake mouse (Fig. 1B). In the neuron from the awake animal, spontaneous activity, shown before the onset of the noxious heat, is markedly higher than that in the anesthetized animals. The amplitude of the response is also larger in the neuron from the awake animal.

Group data comparisons quantify the differences in response properties in anesthetized and awake mice (Fig. 1C-E). Spontaneous firing rates were, on average, more than 5 times higher in awake mice (Fig. 1C, Cohen's d 1.09, $p < 10^{-4}$, Table 1). As detailed in Methods, we considered significant responses spiking activity that exceeded the 95th percent confidence interval of the average pre-stimulus firing rate. We computed response magnitude and duration of these significant response epochs. Response magnitudes (computed as spikes per stimulus) were, on average more than 5 times higher in awake mice (Fig. 1D, Cohen's d 1.49, $p = 0.003$, Table 1), compared to those in anesthetized mice. Response durations were similar in neurons from awake and anesthetized mice (Fig. 1E, $p > 0.99$, Table 1). These findings indicate that spontaneous activity and responses to nociceptive stimuli in parabrachial neurons of naïve mice are substantially different in awake mice, compared to anesthetized mice.

Neuropathic pain is associated with hyperactivity of parabrachial neurons in awake animals

We, and others, have shown—in anesthetized rodents—that the activity of parabrachial neurons is amplified in models of chronic pain (Matsumoto et al., 1996; Uddin et al., 2018; Raver et al., 2020). We tested whether similar changes occur also in awake animals. As in our previous studies (Uddin et al., 2018; Raver et al., 2020), we used the chronic constriction injury of the infraorbital nerve (CCI) model, developed by Bennet and Xie (1988), to induce persistent pain-like behaviors. We tested mechanical hypersensitivity of the face in head restrained mice using a modified version of the "up-down method" (Chaplan et al., 1994) (see Methods). In each of the four animals with CCI, mechanical withdrawal thresholds were lower than in pre-CCI levels (Fig. 3A), indicating that the mice experienced increased tactile hypersensitivity. These changes were recorded between 8 and 56 days after CCI surgery. To assess ongoing pain, we used the mouse grimace scale (MGS) (Langford et al., 2010; Akintola et al., 2017). MGS scores were higher in mice after CCI, relative to controls, and remained higher for as long as they were recorded (up to 8 weeks) (Fig. 3B), suggesting that CCI mice were exhibiting persistent, ongoing pain.

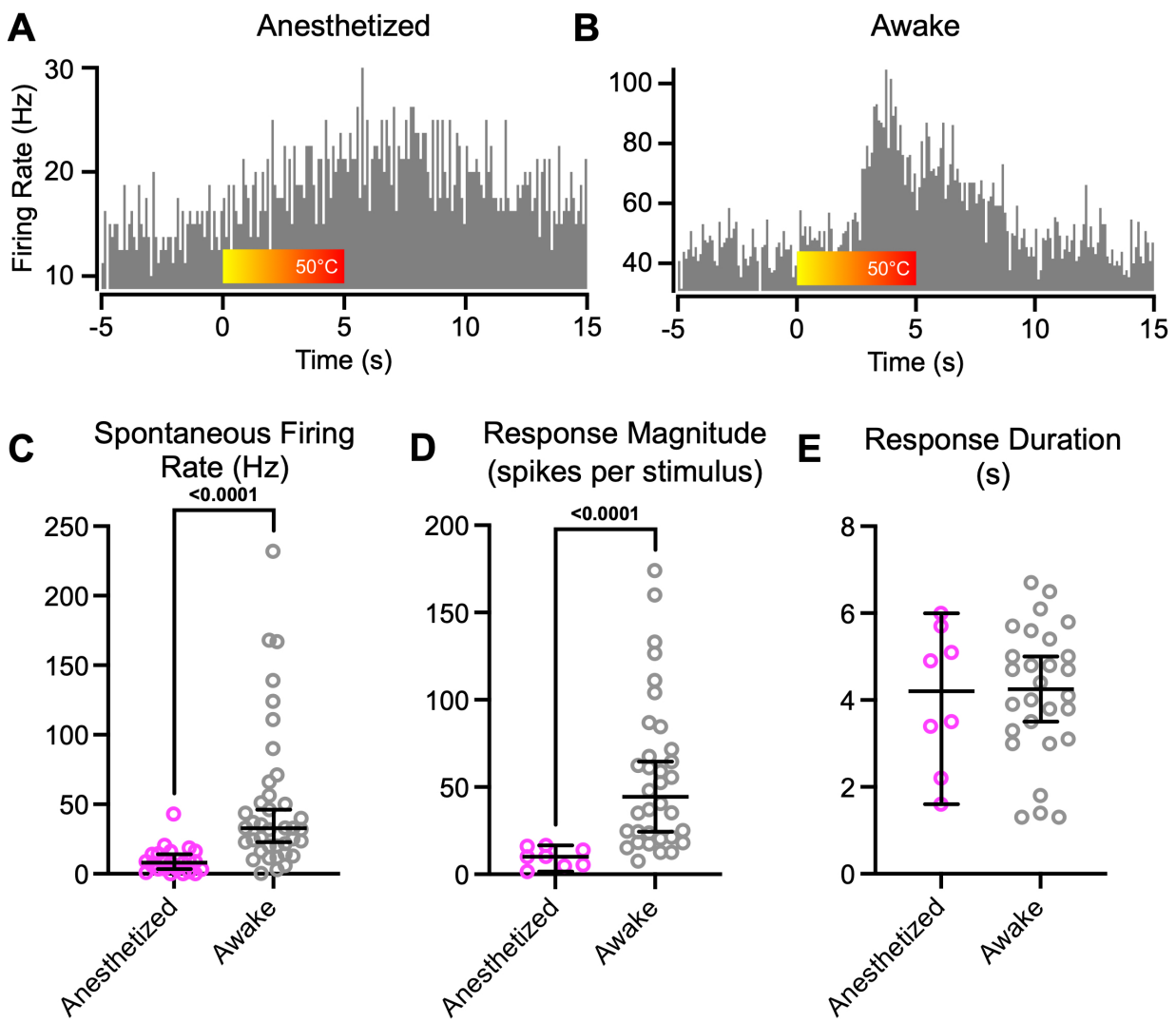

Figure 1: Parabrachial neurons in anesthetized mice respond substantially differently than in awake animals.

A: PSTHs recorded from parabrachial neurons in a urethane-anesthetized and awake (**B**) mice. Color bar indicates application of heat from a laser, producing temperatures that peak at 50°C. Note different y-axes scales. **C:** Spontaneous firing rates and magnitude of responses to noxious heat applied to the face (**D**) were higher in awake mice (Mann-Whitney $U = 109.5$, $p <$ 10-4 and $U = 13$, $p <$ 10-4). **E:** Response durations were indistinguishable in awake and anesthetized mice. Data are medians and 95% confidence intervals.

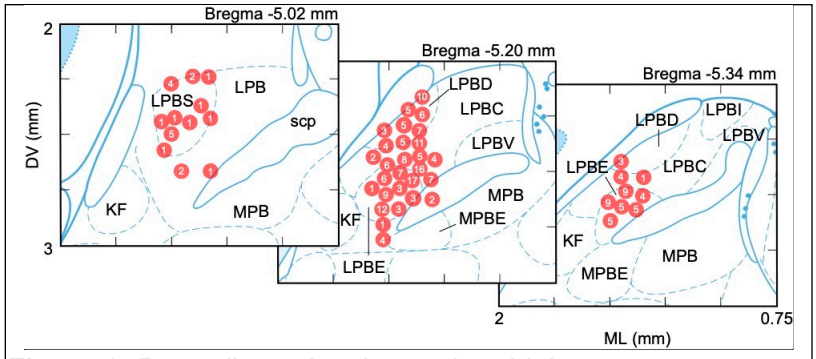

Figure 2: Recordings sites in parabrachial.
Locations of recording sites, derived from stereotaxic coordinates, indicated by red markers. Numbers indicate the number of recordings from the same location. Kölliker-fuse nucleus (KF), lateral parabrachial nucleus (LPB), dorsal part of the lateral parabrachial nucleus (LPBD), central part of the lateral parabrachial nucleus (LPBC), external part of the lateral parabrachial nucleus (LPBE), internal part of the lateral parabrachial nucleus (LPBI), superior part of the lateral parabrachial nucleus (LPBS), ventral part of the lateral parabrachial nucleus (LPBV), medial parabrachial nucleus (MPB), external part of the medial parabrachial nucleus (MPBE), superior cerebellar peduncle (scp). Image maps from Paxinos & Franklin, 2019.

We compared recordings of well isolated, single units from parabrachial in the same mice before and after CCI. There were distinct changes in the response magnitude and duration, but not the spontaneous activity, of parabrachial neurons after CCI. Figure 3 shows an example of peri-event rasters and peri-event histograms recorded from individual parabrachial neurons in the same animal before (Fig. 3C) and 7 days after CCI (Fig. 3D). The neuron recorded after CCI showed an increase in both the magnitude and the duration of responses to heat stimuli applied to the face. In this neuron, spontaneous activity is also higher after CCI, however, when averaged across animals, spontaneous activity did not change after CCI (see below). The neurons recorded before CCI began responding at approximately 45ºC, presumably the nociceptive threshold. In contrast, the neuron recorded after CCI began to fire at temperatures well below noxious threshold, at approximately 30ºC (Fig. 3C and D). Before CCI, all neurons from all animals responded only to nociceptive temperatures; after CCI, all neurons displayed “allodynia”, responding to innocuous temperatures.

We quantified the differences in response properties before and after CCI for each of the mice (Fig. 3E-G). We include, as post-CCI data, neurons recorded from two to eight weeks after CCI, a period in which all animals displayed tactile hypersensitivity and increased MGS scores. We then pooled neurons recorded all animals to compare grouped parabrachial neuronal responses before and after CCI. There was no difference in spontaneous firing rates after CCI in any of the animals (Fig. 3E), but there was an increase in the magnitude of the response (Fig. 3G, Table 1) and response duration (Fig. 3F, Table 1). The magnitude of the responses were 3 times larger after CCI (Fig. 3G, effect size 0.5, $p < 10^{-4}$) and response durations were 3.25 times longer (Fig. 3F, effect size 0.5, $p < 10^{-4}$). Median response duration after CCI was 10.5 sec, far outlasting the duration of the stimulus. These prolonged responses are defined as after-discharges (Matsumoto et al., 1996, Uddin et al., 2018; Raver et al., 2020). The increase in response duration is consistent with our previous findings, in anesthetized rodents, demonstrating that chronic pain is associated with an increase in the incidence and duration of after-discharges in parabrachial neurons (Uddin et al., 2018; Raver et

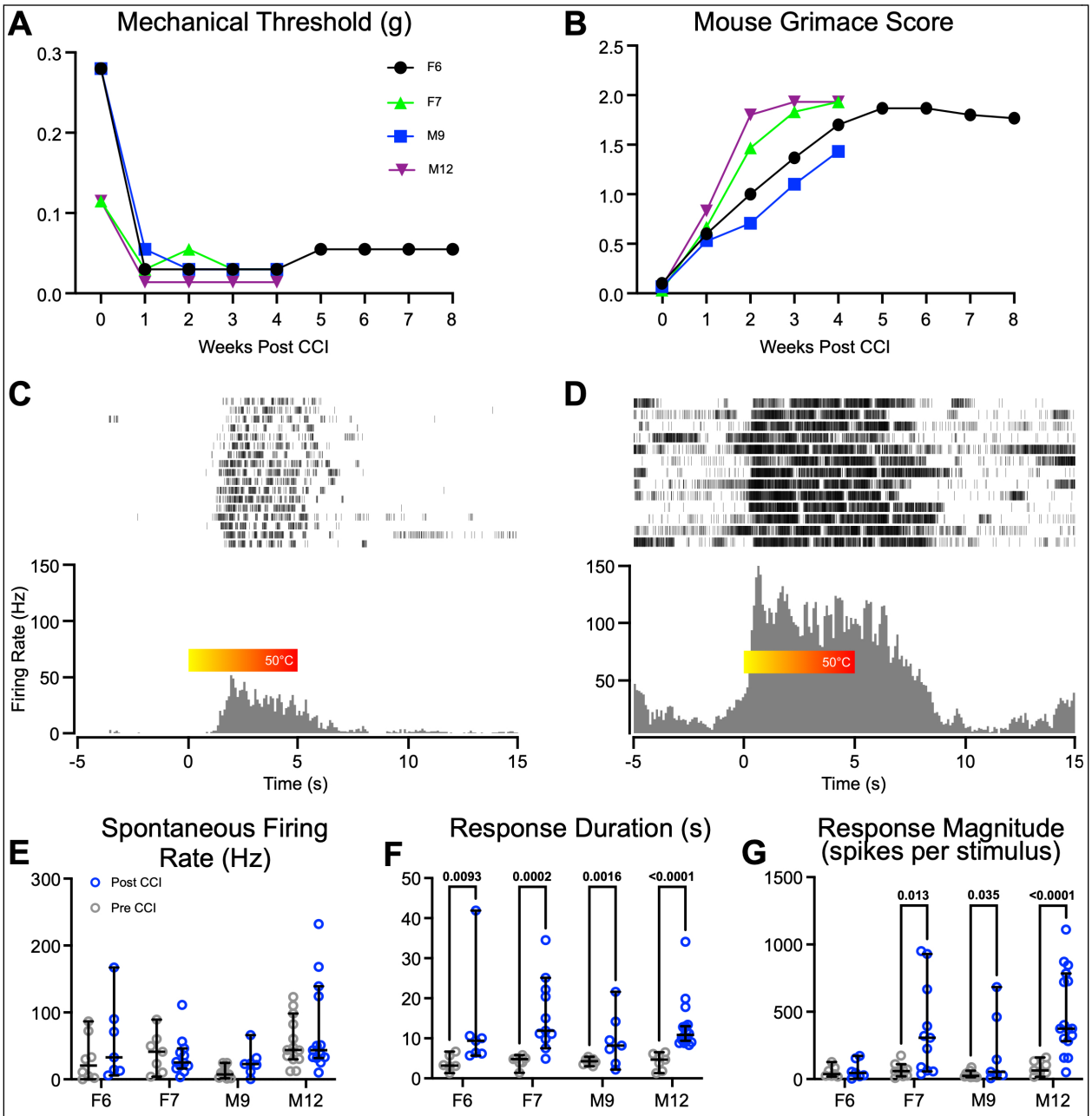

Figure 3: Neuropathic pain is associated with hyperactivity of parabrachial neurons in awake animals.
Time course of reductions in facial tactile hypersensitivity (**A**) and increases in mouse grimace scores (**B**) in each of the four mice (M=male; F=female), after CCI. Representative raster plots and PSTHs of neurons recorded from the same animal before (**C**) and after (**D**) CCI, in response to noxious heat applied to the snout. Color bar shows the increase in heat from room temperature to 50ºC. In each of the mice spontaneous activity was not affected after CCI (**E**), whereas response durations (**F**) and magnitudes (**G**) increased. Data represent medians and 95% confidence intervals; p-values derived from Mann-Whitney tests.

al., 2020). The present data show that, for at least 6 and up to 8 weeks after CCI, there is long lasting amplification of parabrachial neuron activity.

We investigated sex differences by pooling 90 neurons recorded from 8 animals (4 of each sex). In naïve animals, there were no sex differences in spontaneous activity (p = 0.4, median (males)= 24.65, CI (males) = 20.51,42.72; median (females) = 29.95, CI (females) = 24.38,38.66), response duration (p = 0.84, median (males) = 4.8, CI (males) = 7.767, 20.94; median (females) = 5.3, CI (females) = 7.971, 17.63) or response magnitude (p = 0.9, median (males) = 37.95, CI (males) = 53.29, 166.6; median (females) = 35.05, CI (females) = 41.97, 76.39). Similarly, there were no sex differences after CCI in spontaneous activity (p = 0.34, median (males) = 32.45, CI (males) = 28.57, 77.52; median (females) = 25.9, CI (females) = 22.15, 62.45), response duration (p = 0.97, median (males) = 10.2, CI (males) = 10.09, 15.25; median (females) = 10.85, CI (females) = 9.53, 19.89), or response magnitude (p = 0.07, median (males) = 371.5, CI (males) = 292, 564.8; median (females) = 154, CI (females) = 108.5, 422.4).

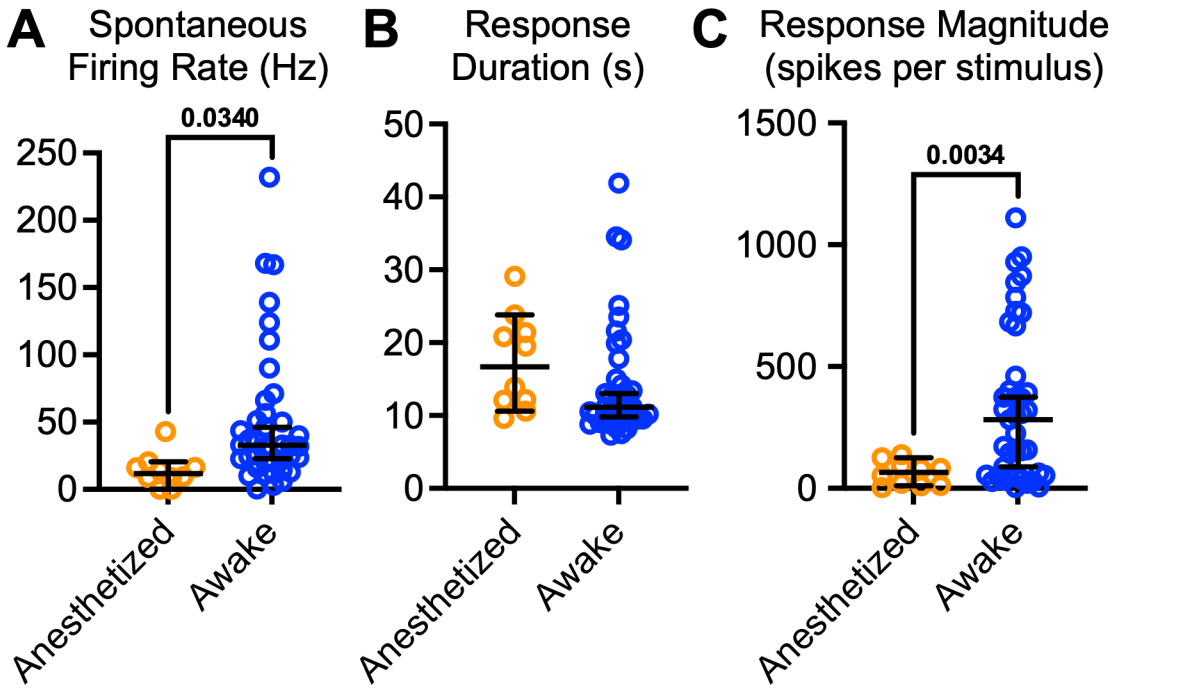

Figure 4: Time course of changes in parabrachial activity after CCI.
Response durations remained elevated for at least 8 weeks post CCI (**A**), and response magnitudes remained elevated for at least 6 weeks (**B**). Purple markers indicated neurons recorded while animals displayed tactile hyperalgesia. Individual data represent individual neurons, and black bars depict weekly median values.

Time-course of changes in parabrachial activity

By recordings from awake animals, we were able to investigate the time course of the activity of parabrachial neurons before and after the induction of chronic pain, and to determine the relationship between the activity of parabrachial neurons and the pain behaviors in individual animals. Figure 4 plots the duration (Fig. 4A) and magnitude (Fig. 4B) of responses in each of the neurons, pooled from the 4 animals, across time. Response duration remained longer than pre-CCI levels for the entirety of the 8 weeks post-CCI period, a period in which the animals experienced hyperalgesia (Fig. 4A). In contrast, response magnitude was elevated relative to pre-CCI levels for at least 6

weeks post-CCI before returning to baseline levels, even though the animals continued to experience hyperalgesia (Fig. 4B).

Anesthesia suppresses the effects of CCI on parabrachial activity

We showed, above, that anesthesia suppresses the responses of parabrachial neurons to acute nociceptive inputs (Fig. 1). We also showed that CCI results in amplification of parabrachial responses, recorded from either awake or anesthetized rodents (Fig. 1). Here, we tested if this amplification is affected by anesthesia. That is, we directly compared parabrachial activity after CCI, in anesthetized *vs* awake mice.

Group data comparisons quantify the differences in responses to noxious heat stimuli in anesthetized and awake mice after CCI (Fig. 5). Spontaneous firing rates were more than 3 times higher in awake mice (Fig. 5A, effect size 4.5, p = 0.03). Response magnitudes were more than 5 times higher in awake mice (Fig. 5C, effect size 5.5, p = 0.003). Response durations were similar in neurons from awake and anesthetized mice (Fig. 5B; $p > 0.99$). These findings indicate that spontaneous activity and responses to nociceptive stimuli in parabrachial neurons of CCI mice are substantially larger in the awake, compared to anesthetized animals, but that the duration of after-discharges is similar in these conditions.

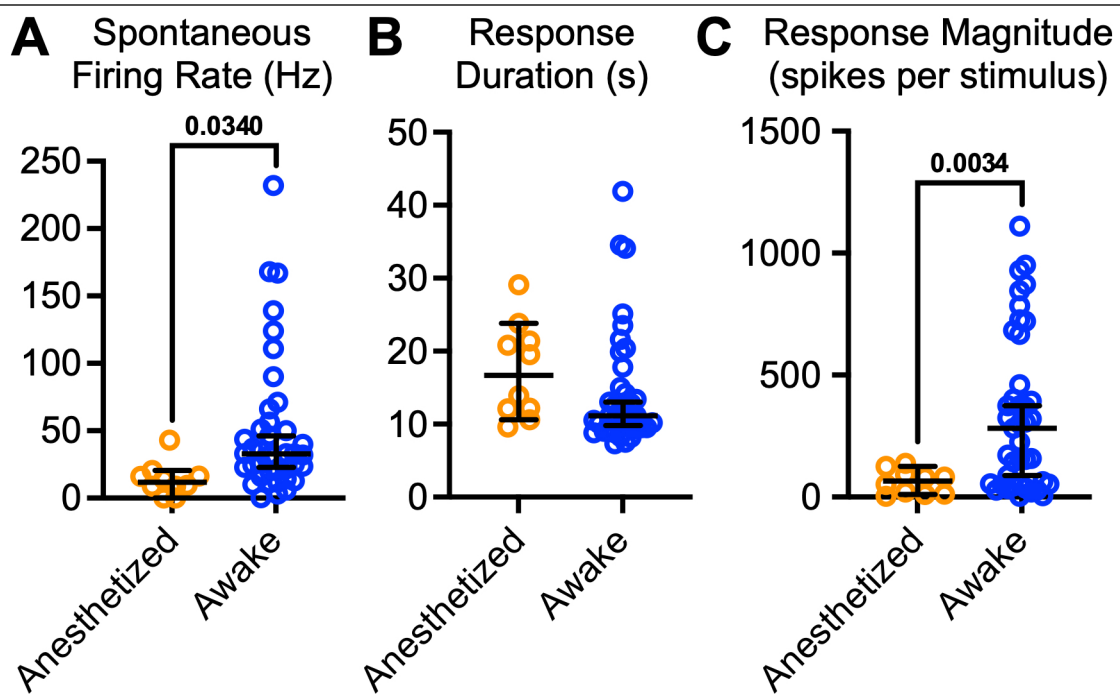

Figure 5: Parabrachial neurons after CCI are substantially different in awake animals. **A**: Post-CCI spontaneous firing rates recorded from awake mice were higher than in anesthetized mice. **B**: There was no difference in response duration in response to noxious heat applied to the face. **C**: Response magnitude was higher in awake mice than in anesthetized mice in response to noxious heat applied to the face. Markers represent cells (n = 10 cells for anesthetized and 44 for awake). Data represent medians and 95% confidence intervals.

Inflammatory pain is associated with hyperactivity of parabrachial neurons in awake animals

To determine if similar changes in parabrachial activity occur also in other models of pain, we induced, in a separate group of animals, inflammatory pain by injection of complete Freund's adjuvant (CFA) in the snout. We assessed tactile hypersensitivity levels at the snout daily on each of the 3 days before CFA injections, and on days 2 to 6 after injections. After CFA, mechanical thresholds decreased (Fig. 6A) indicating that the mice were experiencing increased tactile hypersensitivity.

Between 2 and 6 days after CFA application, there were changes in the spontaneous and evoked activity of parabrachial neurons. Figure 6 depicts an example of peri-event rasters and peri-event histograms recorded from individual parabrachial neurons in the same animal before (Fig. 6B) and after CFA (Fig. 6C). After CFA, there were increases in spontaneous activity, response duration, and response magnitude in all animals tested.

We quantified the differences in response properties before and 6 days after CFA in each of the awake mice (Fig. 6D-F). Unlike in CCI animals, there was an increase in spontaneous firing rates after CFA (Table 1). Neurons from all animals were pooled into pre and post CFA groups, revealing an average 3.3-fold increase in spontaneous activity (Fig. 6D, effect size 0.49, $p < 10^{-4}$), shown before the onset of the noxious heat. 17The increase in spontaneous activity may reflect the persistent inflammatory nature of CFA pain, which may not be as prominent in animals with CCI. Just as with the CCI animals, response durations were 2.7 times longer (Fig. 6E, effect size 0.49, $p < 10^{-4)}$ and response magnitudes were 2.7 times larger after CFA (Fig. 6F, effect size 0.52, $p < 10^{-4}$) in all animals tested, indicating the presence of amplified after discharges. Taken together with the CCI data, these data indicate that mouse models of both chronic neuropathic pain (CCI) and inflammatory pain (CFA) are associated with hyperactivity of parabrachial neurons in awake mice.

We investigated sex differences by pooling 42 neurons recorded all 4 animals (2 males and 2 females). In animals recorded after CFA injections, there were no differences in spontaneous activity (p = 0.59, median (males) = 51.7, CI (males) = 43.94, 100.7; median (females) = 61.9, CI (females) = 51.64, 98.86), response duration (p = 0.13, median (males) = 12.3, CI (males) = 10.54, 16.21; median (females) = 10.7, CI (females) = 10.04, 11.94), or response magnitude (p = 0.92, median (males) = 432.4, CI (males) = 307.8, 662.3; median (females) = 340, 566.9).

The activity of PB^{CGRP} neurons is amplified in inflammatory pain in males

Parabrachial neurons that respond to nociceptive stimuli, and whose activity is related to chronic pain conditions, are in the external lateral portion of the parabrachial nucleus (Uddin et al., 2018; Raver et al., 2020). Many neurons in this region express calcitonin gene-related peptide (CGRP), a peptide implicated in aversive behaviors, including pain (Campos et al., 2018; Chiang et al., 2020; Palmiter, 2018). However, it is not known if amplified activity in persistent pain conditions occurs specifically in parabrachial neurons that express CGRP (PB^{CGRP} neurons). To test this, we used *in vivo* calcium

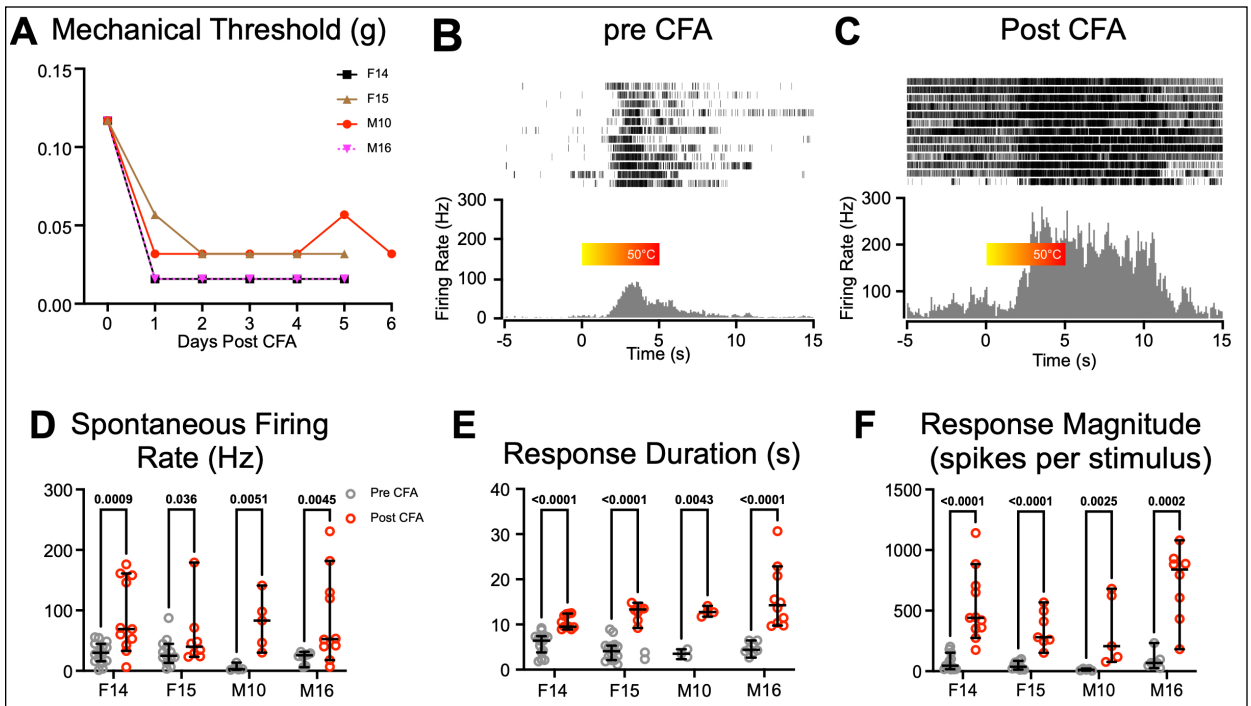

Figure 6: Inflammatory pain is associated with hyperactivity of parabrachial neurons in awake animals.
A: Time course of reductions in facial tactile hypersensitivity in each of the four mice (M=male; F=female), after CFA injection. Representative rasters and PSTHs computed for neurons recorded from the same animal before (**B**) and after (**C**) CFA injection, in response to noxious heat applied to the snout for 5 seconds. The color bar shows the increase in heat from room temperature to 50ºC. **D**: Spontaneous firing rates increased in 3 out of the 4 animals after CFA injections. Both response duration (**E**) and magnitude (**F**) increased after CFA in each of the animals. Data represent medians and 95% confidence intervals.

imaging with fiber photometry to record, from the same animals, population activity of PB^{CGRP} neurons before and after the induction of inflammatory pain (Fig. 7). We produced inflammatory pain by injecting CFA in the snout. We tested mechanical hypersensitivity daily in head restrained mice using a modified version of the “up-down method” (see Methods).

Figures 7A-D depict examples of heat stimulus-evoked calcium indicator responses recorded, in the same animal, before, and 4 days after CFA injections in a male and in a female animal. The portions of the responses that exceed the 95% confidence interval above the mean baseline levels, indicated by the dotted horizontal lines, were defined as significant and labeled in green. The color bar shows the increase in heat, from room temperature to 50°C, which is just above the heat pain threshold for these animals. Note the increase in both response magnitude and duration after CFA, demonstrating amplified activity specifically in PB^{CGRP} neurons.

Figure 7E depicts the time course of changes in the duration of evoked calcium signals recorded from PB^{CGRP} neurons in each of 10 mice (5 females). The horizontal dotted lines depict the 95th percent confidence interval of the mean, pre-CFA activity duration. In all

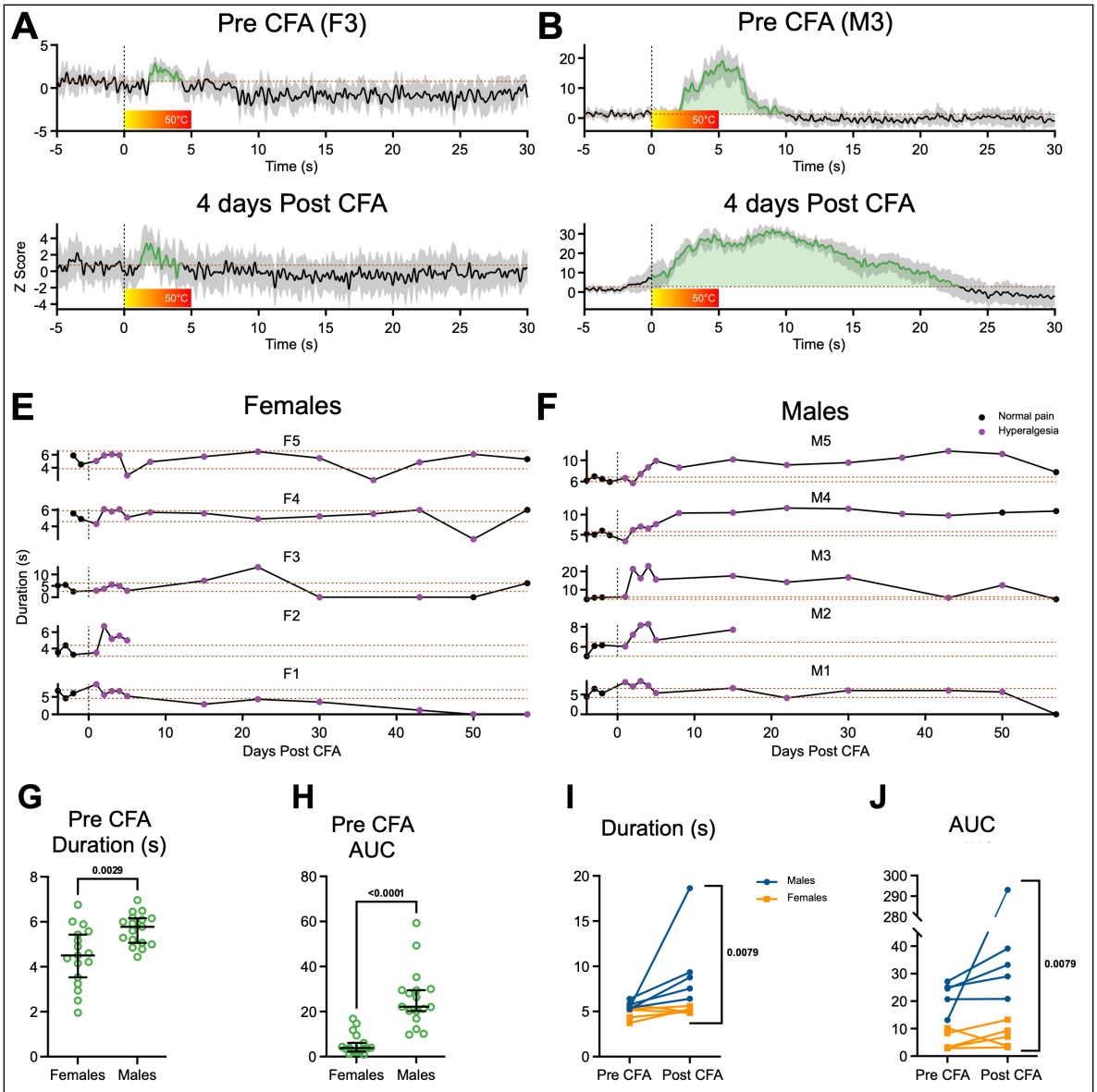

Figure 7: Activity of PBCGRP neurons is amplified in inflammatory pain.
Representative population GCaMP transients recorded, via fiber photometry, from PBCGRP neurons in the same mouse, in response to a 5 second noxious heat applied to the snout before (**A**) and after CFA (**B**) in males and females (**C,D**). Color bar shows the increase in heat from room temperature to 50ºC. The portions of the responses that exceed the 95% confidence interval above the mean baseline levels, indicated by the dotted horizontal lines, were defined as significant and labeled in green. Daily response durations for each animal for both males (**F**), right, and females (**E**), left. The 95% confidence interval is indicated by the dotted horizontal lines. An animal was considered to display mechanical hypersensitivity when its mechanical withdrawal threshold decreased by at least 20% below baseline, indicated by the purple markers. Before CFA injections, males had larger response magnitudes, measured using area under the curve (AUC) (**H**) and larger response durations (**G**), compared to females. After CFA injections, males had larger response durations (**I**) and larger response magnitudes (**J**) compared to females. Data are means and 95% confidence intervals (A to D). Data points are recording sessions with the median and 95% confidence intervals marked (G,H). Data are average pre CFA recordings sessions and up to 5 days post CFA recordings sessions (I,J).

but one **male** animal (M1), PB^{CGRP} response durations increased significantly within 48 hours after CFA injections and remained elevated for at least 40 days, largely paralleling the duration of tactile hyperalgesia (Fig. 7E). This is depicted in Figures 7F, where purple markers indicate timepoints in which an animal displayed hyperalgesia, relative to pre-CFA levels. Black markers indicate data from times in which the mechanical withdrawal threshold had returned to baseline.

In contrast, in **female** mice, PB^{CGRP} response durations rarely exceeded pre-CFA levels, despite the fact that females exhibited mechanical hypersensitivity lasting as long as that in males (Fig. 7E)

We used mechanical hypersensitivity as a behavioral readout because the thermal hypersensitivity tests of the face were unreliable, as even 0.1 W power differences in the laser output—the finest differences in power output the laser could produce—resulted in fluctuating behavioral responses. This may be due to the high sensitivity of the face to the thermal stimulation. Mechanical sensitivity tests, on the other hand, produced consistent behavioral responses at each filament level.

The reduction in calcium signals is not likely related to loss of fluorescence responses, because responses to tail-pinch remained stable throughout these recordings (data not shown).

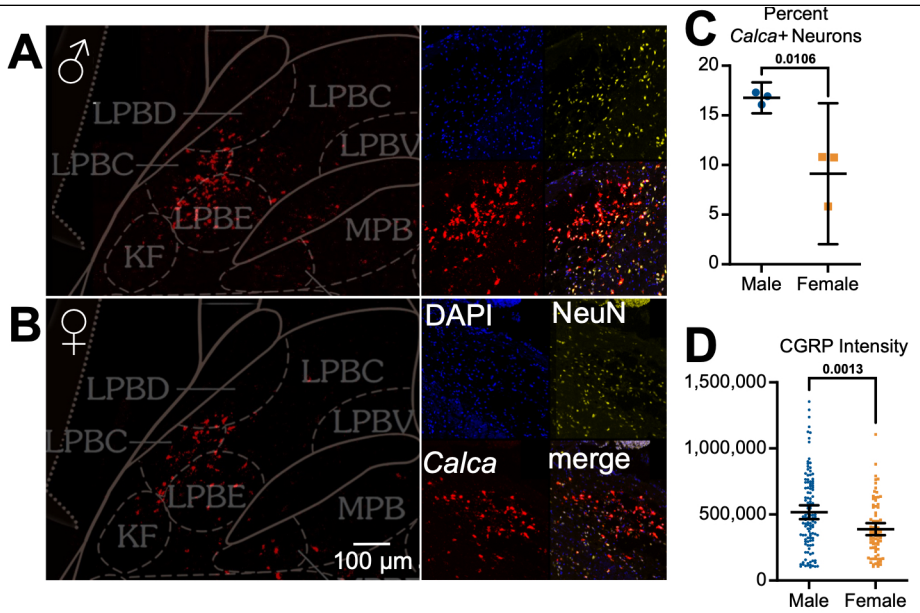

Figure 8: Lateral parabrachial in males has higher Calca expression.
Examples images show more Calca (red) expressed in lateral parabrachial of a male mouse (**A**), compared to a female (**B**). Panels on the right depict separate signals in each channel. To quantify Calca expression, we identified neuronal nuclei (stained for both DAPI+ (blue) and NeuN+ (yellow)), and calculated the percentage of these that expresses Calca. Males (n=3) had a higher percentage of Calca+ neurons, compared to females (n=3; **C**). Neurons in males also had a higher Calca staining intensity (**D**). Means and 95%CI shown. Kölliker-fuse nucleus (KF), dorsal part of the lateral parabrachial nucleus (LPBD), central part of the lateral parabrachial nucleus (LPBC), external part of the lateral parabrachial nucleus (LPBE), ventral part of the lateral parabrachial nucleus (LPBV), medial parabrachial nucleus (MPB).

In **naïve** animals, response magnitudes were larger in males than in females, before CFA injections. In response to noxious heat, response magnitudes in males were 4.7 times larger than in females (Fig. 7H, effect size 2.1, $p < 10^{-4}$) and response durations were 1.3 times larger in males (Fig. 7G, effect size 1.15, $p = 0.0029$). After CFA, response durations were twice longer in males than in females (Fig. 7I, effect size 1.45, $p = 0.008$) and response magnitudes were 11 times larger in males than in females (Fig. 7J, effect size 0.91, $p = 0.008$).

Males express more *Calca* in lateral parabrachial

We tested the hypothesis that the sex differences in responses of PB^{CGRP} neurons to noxious stimuli reflect different expression of CGRP in males and females. We compared RNA expression of *Calca*, the RNA transcript of CGRP. Figure 8A and B depicts micrographs of slices through parabrachial from a male and a female mouse, that were processed for RNAscope. These demonstrate a larger number of labeled cells in the male. We quantified these differences by detecting, using the Imaris system (ssee Methods), cell nuclei that express both the nuclear marker DAPI and the neuronal marker NeuN; these double-labeled nuclei were classified as neuronal nuclei. Neuronal nuclei, as compared to neuronal bodies, were chosen to limit the bias for overestimating relative Calca intensity in larger neurons and the ease in delineating the borders of each region of interest using DAPI. We then identified those neuronal nuclei that expressed *Calca*. This allowed us to determine that, in males, an average of 16.77% (95% CI = 15.21, 18.33) of the neurons in lateral parabrachial were *Calca*+, compared to an average of 9.124% (95% CI = 2.017, 16.23) in females (Fig. 8C, $p = 0.01$, Table1, effect size = 3.69). In the external lateral parabrachial, in males, an average of 46.31% (95% CI = 11.31, 81.32) of the neurons were *Calca*+, compared to an average of 29.8% (95% CI = -10.4, 70). However, in external lateral parabrachial, there was no sex differences ($p = 0.25$). These values are likely an underestimate of the relative *Calca*+ neuronal population in parabrachial because we intentionally reduced the sensitivity of the RNAscope detection to resolve and quantify individual RNA transcripts.

Presumably because of the high expression of *Calca* transcripts (Palmiter 2018) it was not possible to resolve individual transcripts. As an alternative approach, we instead quantified the sum of *Calca* intensity across the neuronal nucleus. This served as a proxy for transcript number, as neurons expressing densely overlaid *Calca*+ puncta appeared brighter and covered a greater proportion of the neuronal area than those expressing sparse *Calca*+ puncta. Only neurons which were considered *Calca*+ were included in further analysis. This allowed us to determine that within *Calca*+ cells, males express more *Calca* than females (Fig. 8D, $p = 0.001$, Table 1, effect size = 0.52). Taken together, these data suggest that the expression of *Calca*, and percent of neurons expressing *Calca*, is higher in lateral parabrachial of males.

Parabrachial activity is correlated with arousal

A benefit of recording from awake animals is the ability to test the hypothesis that parabrachial activity can be modulated by the “behavioral state” of an animal. One approach to assess behavioral states is to measure pupil size as a proxy of the arousal state (de Gee et al., 2020).

Spontaneous activity rates were correlated with pupil size. Figure 9A depicts a representative recording session, plotting changes in both pupil area (blue) and the spontaneous firing rate of a parabrachial neuron (red). Note that pupil dilations appear to immediately precede increases in the neuronal firing rate. Figure 9B quantifies this relationship by plotting instantaneous neuronal firing rates (1 sec bins) against pupil size, demonstrating a positive correlation between these metrics. A significant, positive correlation was seen in 14 out of 17 cells across all 7 animals tested (4 males, 3 females), with r values ranging from 0.55 to 0.12. These findings suggest that arousal states—approximated by changes in pupil diameter—correlate with changes in parabrachial activity.

To determine if arousal states affect evoked responses of parabrachial neurons, we constructed and overlayed PSTHs (0.1 sec bin size) of neuronal activity and pupil size (Fig. 9C). The PSTHs were aligned to the onset of the 5 sec heat stimuli applied to the snout. Pupil dilation and parabrachial activity after the onset of the noxious heat were highly correlated (Fig. 9C,D, r = 0.83, $p = 1.75 \times 10^{-13}$). A significant positive correlation was seen in 13 neurons from 7 animals tested, with r values ranging from 0.9 to 0.5. Four cells had a negative correlation (Fig. 9D). Cross correlation analysis revealed that, in the majority of cells recorded (15 of 17) there was a positive lag, indicating that changes in parabrachial activity preceded changes in pupil size (Fig. 9E).

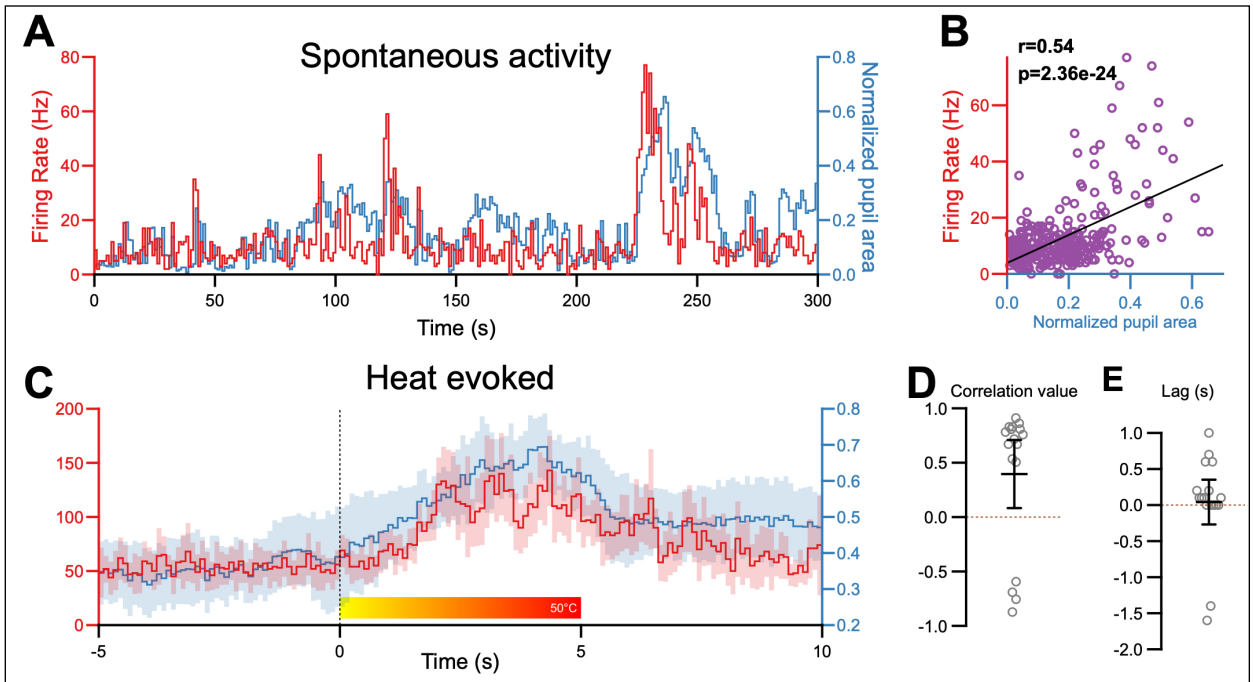

Figure 9: Parabrachial activity is correlated with arousal states.
A: Representative traces depicting spontaneous firing rates (red) of parabrachial neurons and normalized pupil area (blue). **B**: These metrics were positively correlated. **C**: Averaged (and 95% CI) traces of firing rate of parabrachial neurons (red) and pupil area (blue) in response to noxious heat applied to the snout. **D**: The lag-shifted correlation values suggest that firing rate and pupil area changes are positively correlated (n = 17 cells, 7 animals). **E**: The positive lag value after cross-correlation suggests that changes in firing rate preceded changes in pupil area (n = 17 cells, 7 animals).

Auditory conditioning of parabrachial activity

Pairing activation of parabrachial neurons with sucrose produces robust and long-lasting conditioned tase aversion in mice, whereas suppressing parabrachial activity suppresses the acquisition and expression of this conditioned aversion (Chen et al., 2018; Carter et al., 2015). These findings suggest that the activity of parabrachial neurons can be conditioned to respond to innocuous stimuli. To test this, we conditioned head-restrained mice by pairing an auditory tone (1 sec, 100 kHz, 80 dB) with a noxious heat stimulus applied to the snout. We did this while recording from nociceptive neurons in the parabrachial nucleus. Figure 10 depicts an example of one of these recording sessions.

Before conditioning, the parabrachial neuron responded to the heat stimulus (Fig. 9C),

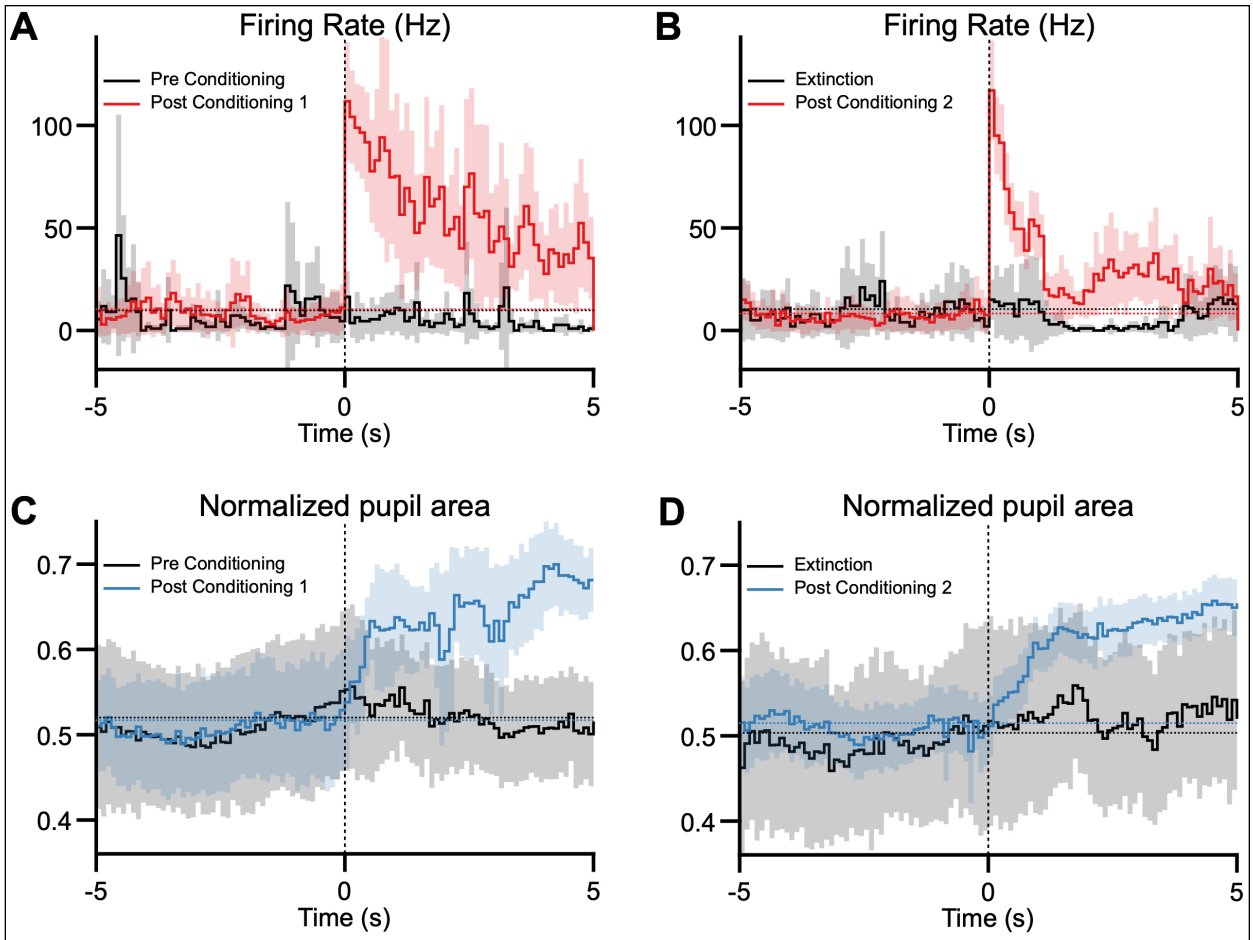

Figure 10: Innocuous auditory conditioning of parabrachial responses.
A: A noxious heat-responsive parabrachial neuron does not respond to an innocuous tone before conditioning (black trace) but responds robustly to the tone after a conditioning (red). **B**: Representative traces showing the same parabrachial neuron undergoing extinction (black), and responses after a second conditioning paradigm (red). **C**: Similarly, pupil responses to the innocuous auditory stimulus appear only after the conditioning paradigm (blue). **D**: Recordings from the same neuron after extinction of the conditioned responses (black trace) and after reconditioning the auditory response (blue). Data represent averages and 95% confidence intervals, indicated by the horizontal dotted lines.

but not to the auditory stimulus (Fig. 10A). We used 15 pairings of auditory tone (1 sec) and heat (5 sec) stimuli, with the auditory stimulus presented 3 seconds after the onset of the noxious heat stimulus, so that the auditory stimulus is presented just before the heat reaches noxious temperatures. After the pairing session, the neuron responded robustly to the auditory tone, and continued to do so for a median of 13 presentations of the tone (delivered every 120 sec; Fig. 10A, range = 16-10 stimuli). After the tone responses extinguished, we delivered a second session of 15 pairings of the auditory tone and heat stimuli, after which the neuron again began responding to the auditory stimulus, and did so for the next 14 stimuli, until this auditory response extinguished (Fig. 10B, median = 13.5 stimuli, range = 20-9 stimuli). Sham pairings (see methods; “unconditioned tone”), where the auditory tone was presented without the noxious heat stimulus, had no effect on parabrachial activity (Fig. 10, grey traces).

We conditioned nociceptive parabrachial neurons to auditory stimuli in 24 neurons from 7 animals (4 males, 3 females), using the conditioning paradigm described above while measuring pupil size changes. None of these neurons responded to auditory stimuli before conditioning, and all of them began responding to the auditory stimuli after conditioning. Significant responses to auditory stimuli could be evoked for 6 to 22 stimuli (median =13) after the conditioning. All the neurons could be conditioned again after extinction of the auditory stimuli. Pupil size significantly increased after the conditioning paradigm in 10 out of the 14 neurons recorded (Fig 10C,D). These data suggest that parabrachial neurons that respond to noxious heat stimuli can be conditioned to respond to an innocuous auditory tone.

Discussion

Anesthesia alters properties of parabrachial neurons

Much of what we know about the neurophysiology of nociception and pain originates from studies using anesthetics. This is unfortunate because anesthesia profoundly alters neuronal responses to noxious stimuli. Some anesthetics nearly completely suppress responses of parabrachial neurons (Luo et al., 2018; Melonakos et al., 2021). We and others have found that parabrachial neurons do respond to noxious stimuli under urethane anesthesia (Bernard and Besson, 1990; Uddin et al., 2018; Raver et al., 2020; Uddin et al., 2021). Here we show that those responses are different from the ones recorded in awake animals: In awake animals, spontaneous parabrachial neuronal activity is, on average, 13 times higher and parabrachial responses to noxious stimuli are, on average, 4 times larger in amplitude than those in urethane anesthetized animals. In contrast, response duration was indistinguishable in awake and anesthetized animals. These findings suggest careful consideration of results obtained from anesthetized or awake animals.

Parabrachial activity correlates with internal states

Recordings from awake animals are required to determine how “internal states” might affect parabrachial activity and pain perception. Internal states directed towards distractions, such as cognitively demanding tasks, can affect pain perception. Detection of a noxious stimulus is compromised while performing a working memory-intensive task (Buhle and Wager, 2010). Inflammatory pain is attenuated in states of hunger, through a process involving neuropeptide Y (NPY) signaling (Alhadeff et al., 2018); manipulating NPY in parabrachial can mimic hunger states, suggesting a role of parabrachial in this state-dependent pain modulation. Similarly, suppressing parabrachial activity inhibits arousal (Kaur et al., 2017), whereas activating parabrachial neurons increases arousal (Kaur and Saper, 2019).

We found a direct correlation between parabrachial activity and arousal, as measured by pupil size, during presentation of a noxious stimulus. Since changes in parabrachial activity preceded changes in pupil size, parabrachial activity may be influencing internal states. A potential concern is that thermal stimulation may directly lead to pupil dilation, independent of central mechanisms. This is because thermal stimulation of the snout activates the V1 branch of the trigeminal nerve (Kim et al., 2014), potentially causing pupil dilation via the ciliary nerve, which contains fibers from the V1 branch of the trigeminal nerve (Joo et al., 2014; McDougal and Gamlin, 2016). However, our finding that pupil size and parabrachial activity are correlated in the absence of heat stimuli argues against this possibility.

Nociceptive parabrachial neurons can be conditioned to respond to an auditory tone

In addition to its role in nociception and arousal, the parabrachial is also involved in aversive behaviors. For example, stimulating the parabrachial induces conditioned taste aversion, whereas silencing it attenuates conditioned taste aversion (Carter et al., 2015, Chen et al., 2018). Optogenetic stimulation of the parabrachial nucleus induces context-dependent freezing, demonstrating its involvement with threat memory and fear

conditioning (Han et al., 2015; Campos et al., 2018; Bowen et al., 2020). Although these studies show that parabrachial neurons are necessary and sufficient for fear conditioning, they do not elucidate the underlying function of specific parabrachial neurons. We found that the same parabrachial neurons that respond to noxious stimuli can be conditioned to respond to non-noxious stimuli. Changes in pupil size mirrored this conditioned behavior. These findings suggest that conditioned aversion may involve plasticity in the response properties of parabrachial neurons, consistent with evidence for a causal role of the parabrachial in conditioned aversive behaviors (Carter et al., 2015; Campos et al., 2018; Chen et al., 2018; Bowen et al., 2020).

The auditory-nociceptive conditioning paradigm in our study evoked short-lasting conditioning of both pupil dilation responses and parabrachial responses to the conditioned auditory stimuli (Fig. 10). In contrast, conditioned aversion induced by pairing direct stimulation of the parabrachial with tastants, or pairing tastants with appetite-suppressing substances, produced aversive behaviors that can last days (Carter et al., 2015; Campos et al., 2018; Chen et al., 2018; Bowen et al., 2020). A causal role for the parabrachial in this long-lasting aversion is supported by finding that suppressing parabrachial activity attenuates the conditioned behavior (Carter et al., 2015; Campos et al., 2018; Chen et al., 2018; Bowen et al., 2020).

Our findings (shown in Fig. 10) confirm that individual parabrachial neurons can respond to multiple modalities (Sammons et al., 2016; Campos et al., 2018; Bowen et al., 2020), including to nociceptive stimuli (Kang et al., 2022). It has been shown that individual parabrachial neurons respond during the conditioning phase, where a noxious stimulus is paired with a non-noxious tone, but they did not respond when presented with the conditioned tone 24 hours later (Kang et al., 2022). Our findings show that the same parabrachial neurons that respond to noxious heat can be rapidly conditioned to respond to an auditory tone, confirming that parabrachial neurons may be responsible for aversive memory formation. However, we also show that this conditioned response is short lived, lasting only up to one hour after conditioning, suggesting that parabrachial neurons may be involved in short term aversive memory retrieval but not in long term aversive memory retrieval.

PB^{CGRP} neurons respond differently to pain in males and females

Parabrachial neurons expressing calcitonin gene-related peptide (CGRP) have been implicated in driving pain behaviors. Inhibition of PB^{CGRP} neurons attenuates pain behaviors (Han et al., 2015). PB^{CGRP} neurons are also involved in acute pain perception, as they respond to acute noxious stimuli (Campos et al., 2018; Kang et al., 2022). One study reported that CGRP application in parabrachial can produce analgesia, and that this effect is blocked by sub-nanomolar concentrations of a CGRP antagonist (Wang et al., 2021). To our knowledge, this is the only report suggesting that CGRP might be anti-nociceptive. In contrast, we found that PB^{CGRP} neurons respond to nociceptive stimuli, and that, in males, their activity increased after inflammatory pain.

Our results suggest that PB^{CGRP} neurons may play a different role in males and in females. In naïve animals, in response to noxious heat, PB^{CGRP} neurons showed a larger response magnitude and duration. Further, we found that CGRP RNA expression in lateral parabrachial is higher in males than in females.

In our inflammatory pain model (CFA), changes in the activity of PB^{CGRP} neurons—measured with calcium imaging photometry—were also sex-specific. The activity of these neurons increased after the induction of persistent pain in males, but not in females. This increased activity occurred, on average, for 21 days following CFA, after which activity returned to pre-CFA levels. This PB^{CGRP} activity demonstrated divergence from behavioral metrics of pain, as even though both males and females had elevated mechanical hypersensitivity. An important caveat is that we used mechanical hypersensitivity as the behavioral readout, but noxious thermal stimuli to evoke calcium responses. This is because the thermal hypersensitivity tests of the face were unreliable, as described in Results. Using a different modality for the behavioral test may explain why both males and females displayed behavioral hyperalgesia but only males displayed increases in evoked responses after CFA.

By contrast, in both the inflammatory models and in the neuropathic pain models (CCI-ION), single unit recordings reveal sustained elevations in the responses of *individual* parabrachial neurons, lasting for as long as recordings were obtained (8 weeks), in parallel with the sustained mechanical hypersensitivity.

The discordance between the photometry and single unit data may suggest that different populations of PB^{CGRP} neurons display amplified activity during different phases of persistent pain. During the first weeks after persistent pain, the activity of all or most neurons is amplified, as we and others previously reported (Bernard and Besson, 1990; Uddin et al., 2018; Raver et al., 2020). The integrated activity of this large population is accurately reflected in integrated calcium signals recorded through photometry. At later stages, only a subpopulation of PB^{CGRP} neurons might have sustained, amplified firing. Our single unit recordings may be biased toward these hyperactive neurons, whose activity tracks the behavioral hypersensitivity recorded at these later stages. In the photometry recordings, we are recording solely from CGRP neurons while in the single unit recordings, we could be recording from a mixed population of neuronal subtypes. This is unlikely to fully explain these differences as the external lateral parabrachial—the area that we are recording from—expresses CGRP in almost 50% of the cells (Palmiter 2018).

These differences might also reflect the fact that, with photometry, we recorded only from CGRP neurons, whereas single unit recordings may have been from a mixed population of neurons. Throughout this study, the majority of our recordings were from the lateral parabrachial. Because we saw differences in activity, we looked at RNA differences. To our knowledge, only one study quantified CGRP in the parabrachial, exclusively in males (Palmiter 2018). However, in the external lateral parabrachial—the area that we primarily recorded from—a large majority of neurons express CGRP (Palmiter 2018; Huang et al., 2021, Karthik et al., 2022). This suggests that most of our single unit recordings were from CGRP neurons and both recording modalities sample similar neuronal populations.

The difference between our bulk-recording (photometry) and single unit data might be due to females having a smaller population of PB^{CGRP} neurons conveying nociceptive information, a finding consistent with our RNAscope data. Due to the low spatial resolution of fiber photometry, changes in activity in a smaller number of PB^{CGRP} neurons

are harder to detect than in a larger number of neurons. This might also explain the differences in the magnitude of the responses between the males and the females.

It is also possible that, in males, PB^{CGRP} neurons are firing more synchronously than in females. In photometry, this could manifest as a larger calcium transient, due to the higher likelihood of signals from synchronously active neurons to integrate.

The sex differences in CGRP function reported here are consistent with findings in the spinal cord, where CGRP promotes pain plasticity evoked by hyperalgesic priming and by spared nerve injury in female rodents but has a limited impact in males (Paige et al., 2022). Our findings appear to suggest that, in parabrachial, CGRP has a *greater* role in responses of males to both acute and chronic pain. Overall, although CGRP is highly expressed in parabrachial (Palmiter 2018), most of these studies were performed exclusively in males. Future work is necessary to investigate the function of individual PB^{CGRP} neurons.

Table I

Figure	Animal	Metric	Comparison	Test Statistic	Median	P value
1C	N/A	Spontaneous activity	Anesthetized vs awake	Mann-Whitney U = 109.5	Anesthetized= 7.9 Awake= 32.8	$<10^{-4}$
1D	N/A	Response Magnitude	Anesthetized vs awake	Mann-Whitney U = 13	Anesthetized= 10.2 Awake= 44.4	$<10^{-4}$
1E	N/A	Response Duration	Anesthetized vs awake	Mann-Whitney U = 112	Anesthetized= 4.2 Awake= 4.3	>0.99
3E	F6	Spontaneous activity	Pre vs Post CCI	Mann-Whitney U = 18	Pre= 20.5 Post= 32.8	0.28
	M9			Mann-Whitney U = 14	Pre= 7.5 Post= 23.3	0.06
	F7			Mann-Whitney U = 41	Pre= 35.4 Post= 25.2	0.6
	M12			Mann-Whitney U = 56	Pre= 43.9 Post= 35.0	0.7
3F	F6	Response Duration	Pre vs Post CCI	Mann-Whitney U = 3.5	Pre= 3.2 Post= 9.4	0.009
	M9			Mann-Whitney U = 0	Pre= 4.3 Post= 9.5	0.003
	F7			Mann-Whitney U = 3	Pre= 4.4 Post= 11.9	0.0002
	M12			Mann-Whitney U = 0	Pre= 4.7 Post= 10.7	$<10^{-4}$
3G	F6	Response Magnitude	Pre vs Post CCI	Mann-Whitney U = 4	Pre= 24.6 Post= 50.4	0.11

	M9			Mann-Whitney U = 12	Pre= 23.7 Post= 98.7	0.03
	F7			Mann-Whitney U = 17	Pre= 58.9 Post=307.0	0.012
	M12			Mann-Whitney U = 2	Pre= 64.6 Post= 374.0	$<10^{-4}$
5A	N/A	Spontaneous activity	Anesthetized vs awake Post CCI	Mann-Whitney U = 69.50	Anesthetized= 11.8 Awake= 32.8	0.001
5B	N/A	Response Duration	Anesthetized vs awake Post CCI	Mann-Whitney U = 115.5	Anesthetized= 16.7 Awake= 11.2	0.06
5C	N/A	Response Magnitude	Anesthetized vs awake Post CCI	Mann-Whitney U = 85	Anesthetized= 65.7 Awake= 282.0	0.003
6D	M10	Spontaneous activity	Pre vs Post CFA	Mann-Whitney U = 1	Pre= 2.9 Post= 46.7	0.005
	F14			Mann-Whitney U = 25	Pre= 29.8 Post= 70.2	0.001
	F15			Mann-Whitney U = 34	Pre= 28.0 Post= 46.7	0.04
	M16			Mann-Whitney U = 14	Pre= 26.0 Post= 52.0	0.004
6E	M10	Response Duration	Pre vs Post CFA	Mann-Whitney U = 0	Pre= 3.5 Post= 12.5	0.004
	F14			Mann-Whitney U = 3	Pre= 3.9 Post= 9.1	$<10^{-4}$
	F15			Mann-Whitney U = 2	Pre= 2.1 Post=9.2	$<10^{-4}$

	M16			Mann-Whitney U = 0	Pre= 3.8 Post= 9.6	$<10^{-4}$
6F	M10	Response Magnitude	Pre vs Post CFA	Mann-Whitney U = 0	Pre= 11.9 Post=136.0	0.0025
	F14			Mann-Whitney U = 2	Pre= 17.2 Post=354.3	$<10^{-4}$
	F15			Mann-Whitney U = 0	Pre= 36.6 Post=317.5	$<10^{-4}$
	M16			Mann-Whitney U = 1	Pre= 67.6 Post=701.5	0.0002
7I	N/A	Duration	Males vs Females Pre CFA	Mann-Whitney U = 60	Females= 4.5 Males= 5.8	0.003
7J	N/A	AUC	Males vs Females Pre CFA	Mann-Whitney U = 8	Females= 3.8 Males= 22.2	$<10^{-4}$
7K	N/A	Duration	Males vs Females Post CFA	Mann-Whitney U = 0	Females= 4.99 Males= 8.77	0.008
7L	N/A	AUC	Males vs Females Post CFA	Mann-Whitney U = 0	Females= 7.08 Males= 33.71	0.008
8C	N/A	Percent *Calca*+ Neurons	Males vs Females	t = 4.523	Mean: Females= 9.1 Males = 16.8	0.01
8D	N/A	CGRP Intensity	Males vs Females	Mann-Whitney U = 3532	Females= 352107 Males = 473810	0.001
9B	N/A	N/A	Firing rate vs Pupil size correlation	Spearman's r =0.542	N/A	2.4^{-24}

Table 1: Statistics for Figures 1 through 9 showing the corresponding figure number, animals, metric, comparisons being made, test statistic, medians or means, and *p* values.

References

Akintola T, Raver C, Studlack P, Uddin O, Masri R, Keller A (2017) The grimace scale reliably assesses chronic pain in a rodent model of trigeminal neuropathic pain. Neurobiology of Pain 2:13–17.

Alhadeff AL, Su Z, Hernandez E, Klima ML, Phillips SZ, Holland RA, Guo C, Hantman AW, De Jonghe BC, Betley JN (2018) A neural circuit for the suppression of pain by a competing need state. Cell 173:140–152.

Auvray M, Myin E, Spence C (2010) The sensory-discriminative and affective-motivational aspects of pain. Neuroscience & Biobehavioral Reviews 34:214–223.

Bennett GJ, Xie YK (1988) A peripheral mononeuropathy in rat that produces disorders of pain sensation like those seen in man. Pain 33:87–107.

Bernard J, Besson J (1990) The spino (trigemino) pontoamygdaloid pathway: electrophysiological evidence for an involvement in pain processes. Journal of Neurophysiology 63:473–490.

Borsook D (2012) Neurological diseases and pain. Brain 135:320–344.

Bowen AJ, Chen JY, Huang YW, Baertsch NA, Park S, Palmiter RD (2020) Dissociable control of unconditioned responses and associative fear learning by parabrachial CGRP neurons. eLife 9:e59799.

Bruno CA, O'Brien C, Bryant S, Mejaes JI, Estrin DJ, Pizzano C, Barker DJ (2021) pMAT: An open-source software suite for the analysis of fiber photometry data. Pharmacology Biochemistry and Behavior 201:173093.

Buhle J, Wager TD (2010) Performance-dependent inhibition of pain by an executive working memory task. Pain 149:19–26.

Bushnell MC, Čeko M, Low LA (2013) Cognitive and emotional control of pain and its disruption in chronic pain. Nature Reviews Neuroscience 14:502–511.

Cai YQ, Wang W, Paulucci-Holthauzen A, Pan ZZ (2018) Brain circuits mediating opposing effects on emotion and pain. Journal of Neuroscience 38:6340–6349.

Campos CA, Bowen AJ, Roman CW, Palmiter RD (2018) Encoding of danger by parabrachial CGRP neurons. Nature 555:617–622.

Carter ME, Han S, Palmiter RD (2015) Parabrachial calcitonin gene-related peptide neurons mediate conditioned taste aversion. Journal of Neuroscience 35:4582–4586.

Chaplan SR, Bach FW, Pogrel J, Chung J, Yaksh T (1994) Quantitative assessment of tactile allodynia in the rat paw. Journal of Neuroscience Methods 53:55–63.

Chen JY, Campos CA, Jarvie BC, Palmiter RD (2018) Parabrachial CGRP neurons establish and sustain aversive taste memories. Neuron 100:891–899.

Chiang MC, Bowen A, Schier LA, Tupone D, Uddin O, Heinricher MM (2019) Parabrachial complex: a hub for pain and aversion. Journal of Neuroscience 39:8225–8230.

Chiang MC, Nguyen EK, Canto-Bustos M, Papale AE, Oswald AMM, Ross SE (2020) Divergent neural pathways emanating from the lateral parabrachial nucleus mediate distinct components of the pain response. Neuron 106:927–939.

de Gee JW, Tsetsos K, Schwabe L, Urai AE, McCormick D, McGinley MJ, Donner TH (2020) Pupil-linked phasic arousal predicts a reduction of choice bias across species and decision domains. eLife 9:e54014.

de Melo Turnes J, Araya EI, Barroso AR, Baggio DF, de Oliveira Koren L, Zanoveli JM, Chichorro JG (2022) Blockade of kappa opioid receptors reduces mechanical hyperalgesia and anxiety-like behavior in a rat model of trigeminal neuropathic pain. Behavioural Brain Research 417:113595.

Dixon W (1965) The up-and-down method for small samples. Journal of the American Statistical Association 60:967–978.

Fields HL (1999) Pain: An unpleasant topic. Pain 82:S61–S69.

Han S, Soleiman MT, Soden ME, Zweifel LS, Palmiter RD (2015) Elucidating an affective pain circuit that creates a threat memory. Cell 162:363–374.

Huang D, Grady FS, Peltekian L, Laing JJ, Geerling JC (2021) Efferent projections of CGRP/Calca-expressing parabrachial neurons in mice. Journal of Comparative Neurology 529:2911–2957.

Joo W, Yoshioka F, Funaki T, Mizokami K, Rhoton Jr AL (2014) Microsurgical anatomy of the trigeminal nerve. Clinical Anatomy 27:61–88.

Kang SJ, Liu S, Ye M, Kim DI, Pao GM, Copits BA, Roberts BZ, Lee KF, Bruchas MR, Han S (2022) A central alarm system that gates multi-sensory innate threat cues to the amygdala. Cell Reports 40:111222.

Karthik S, Huang D, Delgado Y, Laing JJ, Peltekian L, Iverson GN, Grady F, Miller RL, McCann CM, Fritzsch B et al. (2022) Molecular ontology of the parabrachial nucleus. Journal of Comparative Neurology 530:1658–1699.

Kaur S, Saper CB (2019) Neural circuitry underlying waking up to hypercapnia. Frontiers in Neuroscience 13:401.

Kaur S, Wang JL, Ferrari L, Thankachan S, Kroeger D, Venner A, Lazarus M, Wellman A, Arrigoni E, Fuller PM et al. (2017) A genetically defined circuit for arousal from sleep during hypercapnia. Neuron 96:1153–1167.

Kim YS, Chu Y, Han L, Li M, Li Z, LaVinka PC, Sun S, Tang Z, Park K, Caterina MJ et al. (2014) Central terminal sensitization of TRPV1 by descending serotonergic facilitation modulates chronic pain. Neuron 81:873–887.

Landis SC, Amara SG, Asadullah K, Austin CP, Blumenstein R, Bradley EW, Crystal RG, Darnell RB, Ferrante RJ, Fillit H et al. (2012) A call for transparent reporting to optimize the predictive value of preclinical research. Nature 490:187–191.

Langford DJ, Bailey AL, Chanda ML, Clarke SE, Drummond TE, Echols S, Glick S, Ingrao J, Klassen-Ross T, LaCroix-Fralish ML et al. (2010) Coding of facial expressions of pain in the laboratory mouse. Nature Methods 7:447–449.

Legrain V, Crombez G, Mouraux A (2011) Controlling attention to nociceptive stimuli with working memory. PLOS ONE 6:e20926.

Luo T, Yu S, Cai S, Zhang Y, Jiao Y, Yu T, Yu W (2018) Parabrachial neurons promote behavior and electroencephalographic arousal from general anesthesia. Frontiers in Molecular Neuroscience 11:420.

Matsumoto N, Bester H, Menendez L, Besson J, Bernard J (1996) Changes in the responsiveness of parabrachial neurons in the arthritic rat: an electrophysiological study. Journal of Neurophysiology 76:4113–4126.

McDougal DH, Gamlin PD (2015) Autonomic control of the eye. Comprehensive Physiology 5:439.

Melonakos ED, Siegmann MJ, Rey C, O'Brien C, Nikolaeva KK, Solt K, Nehs CJ (2021) Excitation of putative glutamatergic neurons in the rat parabrachial nucleus region reduces delta power during dexmedetomidine but not ketamine anesthesia. Anesthesiology 135:633–648.

Melzack R, Casey KL (1968) Sensory, motivational, and central control determinants of pain: a new conceptual model. The Skin Senses 1:423–43.

O'Connor AB, Dworkin RH (2009) Treatment of neuropathic pain: an overview of recent guidelines. The American Journal of Medicine 122:S22–S32.

Okubo M, Castro A, Guo W, Zou S, Ren K, Wei F, Keller A, Dubner R (2013) Transition to persistent orofacial pain after nerve injury involves supraspinal serotonin mechanisms. Journal of Neuroscience 33:5152–5161.

Paige C, Plasencia-Fernandez I, Kume M, Papalampropoulou-Tsiridou M, Lorenzo LE, David ET, He L, Mejia GL, Driskill C, Ferrini F et al. (2022) A female-specific role for calcitonin gene-related peptide (CGRP) in rodent pain models. Journal of Neuroscience 42:1930–1944.

Palmiter RD (2018) The parabrachial nucleus: CGRP neurons function as a general alarm. Trends in Neurosciences 41:280–293.

Paxinos G, Franklin KB (2019) The mouse brain in stereotaxic coordinates Academic press.

Price DD (2000) Psychological and neural mechanisms of the affective dimension of pain. Science 288:1769–1772.

Raver C, Uddin O, Ji Y, Li Y, Cramer N, Jenne C, Morales M, Masri R, Keller A (2020) An amygdalo-parabrachial pathway regulates pain perception and chronic pain. Journal of Neuroscience 40:3424–3442.

Sammons JD, Weiss MS, Victor JD, Di Lorenzo PM (2016) Taste coding of complex naturalistic taste stimuli and traditional taste stimuli in the parabrachial pons of the awake, freely licking rat. Journal of Neurophysiology 116:171–182.

Smith BH, Torrance N, Bennett MI, Lee AJ (2007) Health and quality of life associated with chronic pain of predominantly neuropathic origin in the community. The Clinical Journal of Pain 23:143–149.

Smith JG, Elias LA, Yilmaz Z, Barker S, Shah K, Shah S, Renton T (2013) The psychosocial and affective burden of posttraumatic neuropathy following injuries to the trigeminal nerve. Journal of Orofacial Pain 27:293–303.

Stringer C, Pachitariu M, Steinmetz N, Reddy CB, Carandini M, Harris KD (2019) Spontaneous behaviors drive multidimensional, brainwide activity. Science 364:eaav7893.

Treede RD, Apkarian AV, Bromm B, Greenspan JD, Lenz FA (2000) Cortical representation of pain: functional characterization of nociceptive areas near the lateral sulcus. Pain 87:113–119.

Uddin O, Anderson M, Smith J, Masri R, Keller A (2021) Parabrachial complex processes dura inputs through a direct trigeminal ganglion-to-parabrachial connection. Neurobiology of Pain 9:100060.

Uddin O, Studlack P, Akintola T, Raver C, Castro A, Masri R, Keller A (2018) Amplified parabrachial nucleus activity in a rat model of trigeminal neuropathic pain. Neurobiology of Pain 3:22–30.

(US) NAP, editor (2011) Institute of Medicine (US) Committee on Advancing Pain Research, Care, and Education Relieving Pain in America: A Blueprint for Transforming Prevention, Care, Education, and Research.

Wang LL, Wang HB, Fu FH, Yu LC (2021) Role of calcitonin gene-related peptide in pain regulation in the parabrachial nucleus of naive rats and rats with neuropathic pain. Toxicology and Applied Pharmacology 414:115428.

Wu TH, Hu LY, Lu T, Chen PM, Chen HJ, Shen CC, Wen CH (2015) Risk of psychiatric disorders following trigeminal neuralgia: a nationwide population-based retrospective cohort study. The Journal of Headache and Pain 16:1–8.

Zelaya CE, Dahlhamer JM, Lucas JW, Connor EM (2020) Chronic pain and high-impact chronic pain among US adults, 2019.

Figure Legends

Figure 1: Parabrachial neurons in anesthetized mice respond substantially differently than in awake animals.

A: PSTHs recorded from parabrachial neurons in a urethane-anesthetized and awake (**B**) mice. Color bar indicates application of heat from a laser, producing temperatures that peak at 50°C. Note different y-axes scales. **C:** Spontaneous firing rates and magnitude of responses to noxious heat applied to the face (**D**) were higher in awake mice (Mann-Whitney $U = 109.5$, $p < 10\text{-}4$ and $U = 13$, $p < 10\text{-}4$). **E:** Response durations were indistinguishable in awake and anesthetized mice. Data are medians and 95% confidence intervals.

Figure 2: Recordings sites in parabrachial.

Locations of recording sites, derived from stereotaxic coordinates, indicated by red markers. Numbers indicate the number of recordings from the same location. Kölliker-fuse nucleus (KF), lateral parabrachial nucleus (LPB), dorsal part of the lateral parabrachial nucleus (LPBD), central part of the lateral parabrachial nucleus (LPBC), external part of the lateral parabrachial nucleus (LPBE), internal part of the lateral parabrachial nucleus (LPBI), superior part of the lateral parabrachial nucleus (LPBS), ventral part of the lateral parabrachial nucleus (LPBV), medial parabrachial nucleus (MPB), external part of the medial parabrachial nucleus (MPBE), superior cerebellar peduncle (scp). Image maps from Paxinos & Franklin, 2019.

Figure 3: Neuropathic pain is associated with hyperactivity of parabrachial neurons in awake animals.

Time course of reductions in facial tactile hypersensitivity (**A**) and increases in mouse grimace scores (**B**) in each of the four mice (M=male; F=female), after CCI. Representative raster plots and PSTHs of neurons recorded from the same animal before (**C**) and after (**D**) CCI, in response to noxious heat applied to the snout. Color bar

shows the increase in heat from room temperature to 50ºC. In each of the mice spontaneous activity was not affected after CCI (**E**), whereas response durations (**F**) and magnitudes (**G**) increased. Data represent medians and 95% confidence intervals; *p*-values derived from Mann-Whitney tests.

Figure 4: Time course of changes in parabrachial activity after CCI.

Response durations remained elevated for at least 8 weeks post CCI (**A**), and response magnitudes remained elevated for at least 6 weeks (**B**). Purple markers indicated neurons recorded while animals displayed tactile hyperalgesia. Individual data represent individual neurons, and black bars depict weekly median values.

Figure 5: Parabrachial neurons after CCI are substantially different in awake animals.

A: Post-CCI spontaneous firing rates recorded from awake mice were higher than in anesthetized mice. **B:** There was no difference in response duration in response to noxious heat applied to the face. **C:** Response magnitude was higher in awake mice than in anesthetized mice in response to noxious heat applied to the face. Markers represent cells (n = 10 cells for anesthetized and 44 for awake). Data represent medians and 95% confidence intervals.

Figure 6: Inflammatory pain is associated with hyperactivity of parabrachial neurons in awake animals.

A: Time course of reductions in facial tactile hypersensitivity in each of the four mice (M=male; F=female), after CFA injection. Representative rasters and PSTHs computed for neurons recorded from the same animal before (**B**) and after (**C**) CFA injection, in response to noxious heat applied to the snout for 5 seconds. The color bar shows the increase in heat from room temperature to 50ºC. **D:** Spontaneous firing rates increased in 3 out of the 4 animals after CFA injections. Both response duration (**E**) and magnitude (**F**) increased after CFA in each of the animals. Data represent medians and 95%

confidence intervals.

Figure 7: Activity of PBCGRP neurons is amplified in inflammatory pain.

Representative population GCaMP transients recorded, *via* fiber photometry, from PBCGRP neurons in the same mouse, in response to a 5 second noxious heat applied to the snout before (**A**) and after CFA (**B**) in males and females (**C**,**D**). Color bar shows the increase in heat from room temperature to 50ºC. The portions of the responses that exceed the 95% confidence interval above the mean baseline levels, indicated by the dotted horizontal lines, were defined as significant and labeled in green. Daily response durations for each animal for both males (**F**), right, and females (**E**), left. The 95% confidence interval is indicated by the dotted horizontal lines. An animal was considered to display mechanical hypersensitivity when its mechanical withdrawal threshold decreased by at least 20% below baseline, indicated by the purple markers. Before CFA injections, males had larger response magnitudes, measured using area under the curve (AUC) (**H**) and larger response durations (**G**), compared to females. After CFA injections, males had larger response durations (**i**) and larger response magnitudes (**J**) compared to females. Data are means and 95% confidence intervals (**A** to **D**). Data points are recording sessions with the median and 95% confidence intervals marked (**G**,**H**). Data are average pre CFA recordings sessions and up to 5 days post CFA recordings sessions (**I**,**J**).

Figure 8: Lateral parabrachial in males has higher *Calca* expression.

Examples images show more *Calca* (red) expressed in lateral parabrachial of a male mouse(**A**), compared to a female (**B**). Panels on the right depict separate signals in each channel. To quantify *Calca* expression, we identified neuronal nuclei (stained for both DAPI+ (blue) and NeuN+ (yellow)), and calculated the percentage of these that expresses *Calca*. Males (n=3) had a higher percentage of *Calca+* neurons, compared to females (n=3; **C**). Neurons in males also had a higher *Calca* staining intensity (**D**). Means and 95%CI shown. Kölliker-fuse nucleus (KF), dorsal part of the lateral

parabrachial nucleus (LPBD), central part of the lateral parabrachial nucleus (LPBC), external part of the lateral parabrachial nucleus (LPBE), ventral part of the lateral parabrachial nucleus (LPBV), medial parabrachial nucleus (MPB).

Figure 9: Parabrachial activity is correlated with arousal states.

A: Representative traces depicting spontaneous firing rates (red) of parabrachial neurons and normalized pupil area (blue). **B:** These metrics were positively correlated. **C:** Averaged (and 95% CI) traces of firing rate of parabrachial neurons (red) and pupil area (blue) in response to noxious heat applied to the snout. **D:** The lag-shifted correlation values suggest that firing rate and pupil area changes are positively correlated (n = 17 cells, 7 animals). **E:** The positive lag value after cross-correlation suggests that changes in firing rate preceded changes in pupil area (n = 17 cells, 7 animals).

Figure 10: Innocuous auditory conditioning of parabrachial responses.

A: A noxious heat-responsive parabrachial neuron does not respond to an innocuous tone before conditioning (black trace) but responds robustly to the tone after a conditioning (red). **B:** Representative traces showing the same parabrachial neuron undergoing extinction (black), and responses after a second conditioning paradigm (red). **C:** Similarly, pupil responses to the innocuous auditory stimulus appear only after the conditioning paradigm (blue). **D:** Recordings from the same neuron after extinction of the conditioned responses (black trace) and after reconditioning the auditory response (blue). Data represent averages and 95% confidence intervals, indicated by the horizontal dotted lines.

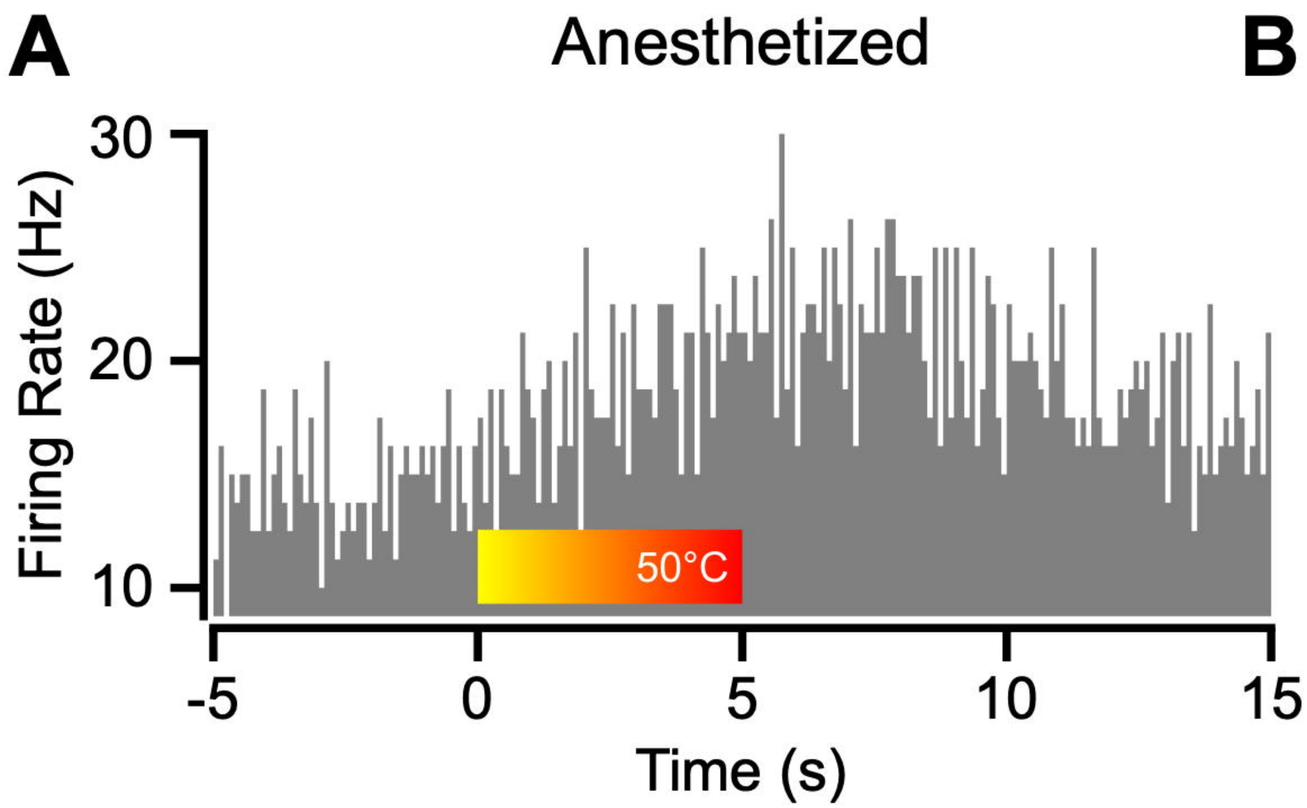
A
Anesthetized
Firing Rate (Hz)
30
20
10
50°C
-5
0
5
10
15
Time (s)

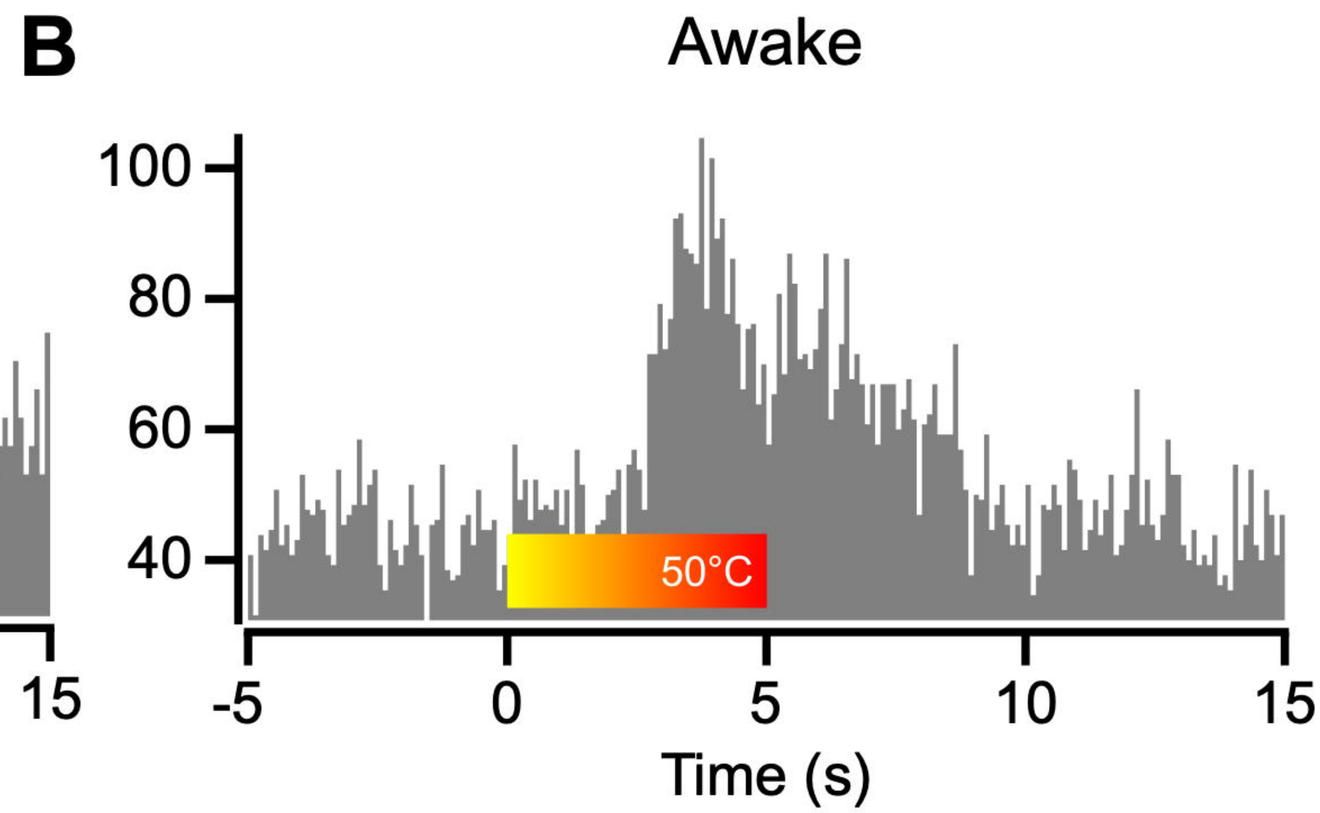
B
Awake
100
80
60
40
50°C
-5
0
5
10
15
Time (s)

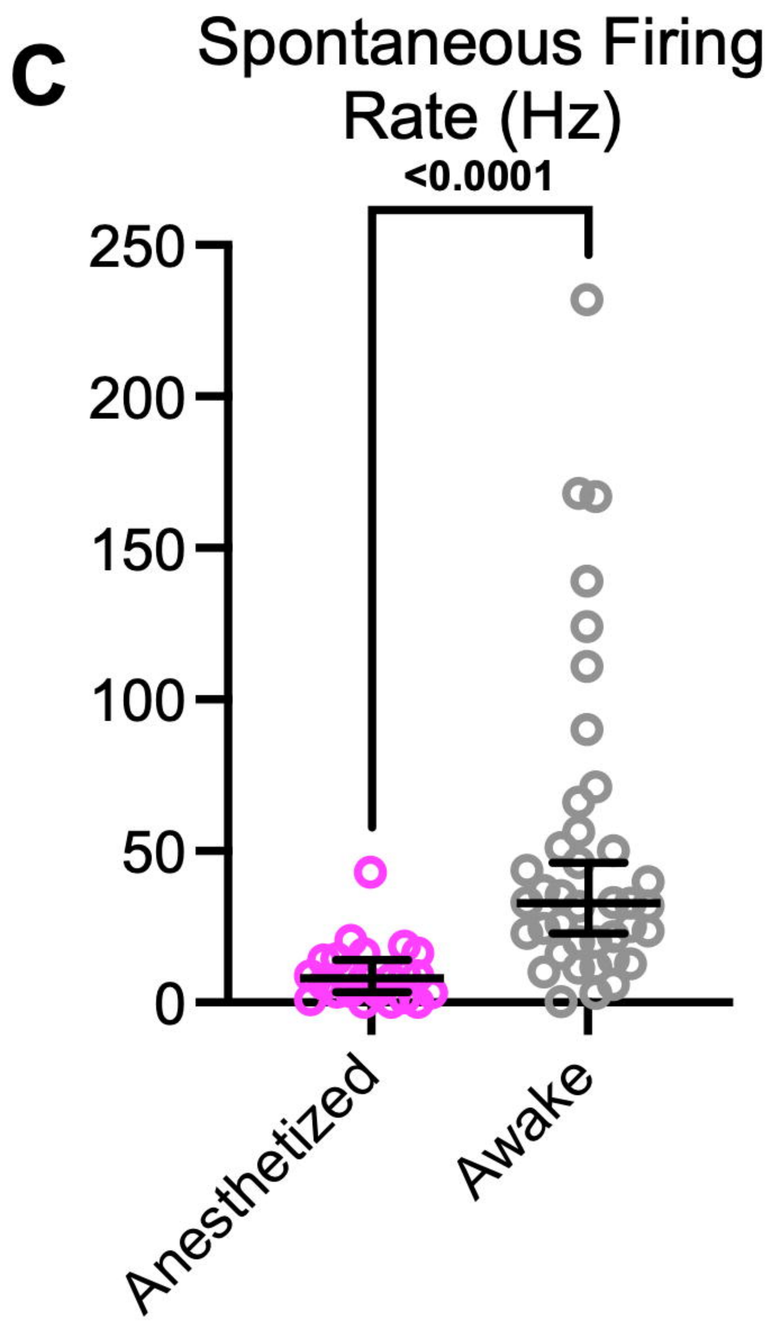
C
Spontaneous Firing Rate (Hz)
<0.0001
250
200
150
100
50
0
Anesthetized
Awake

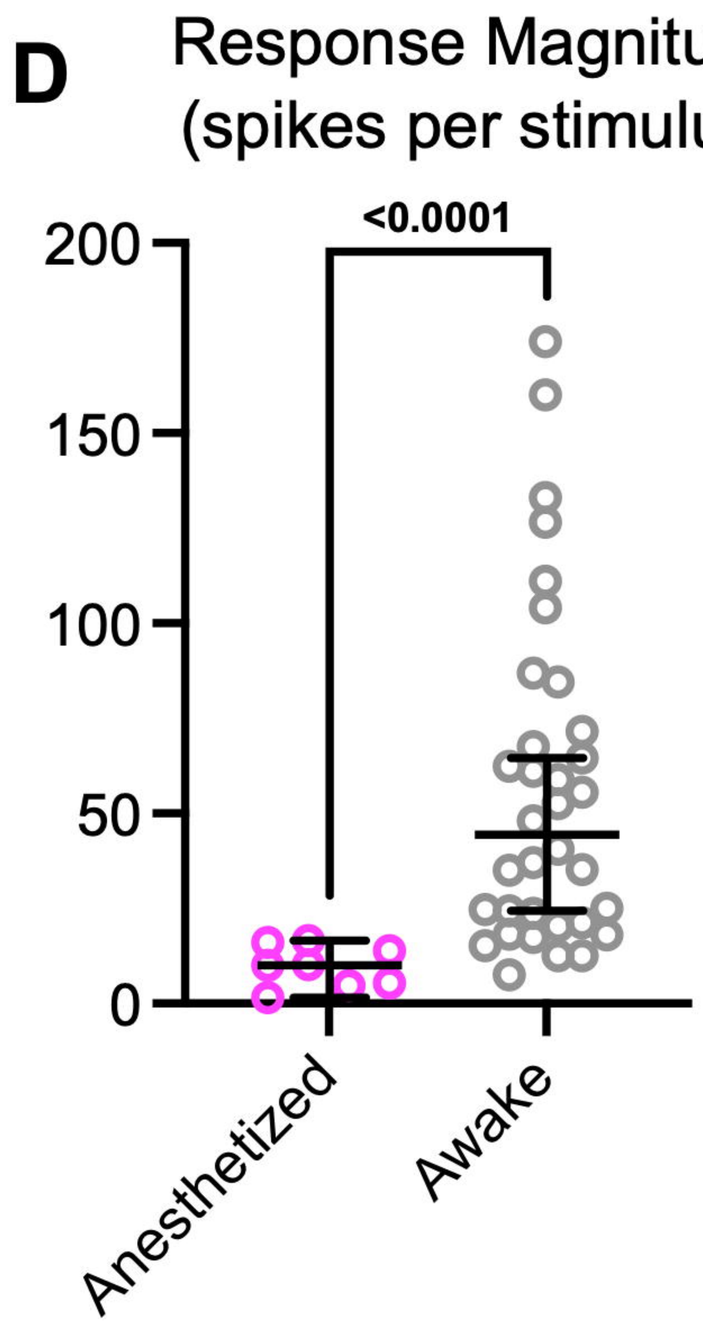
D
Response Magnitude (spikes per stimulus)
<0.0001
200
150
100
50
0
Anesthetized
Awake

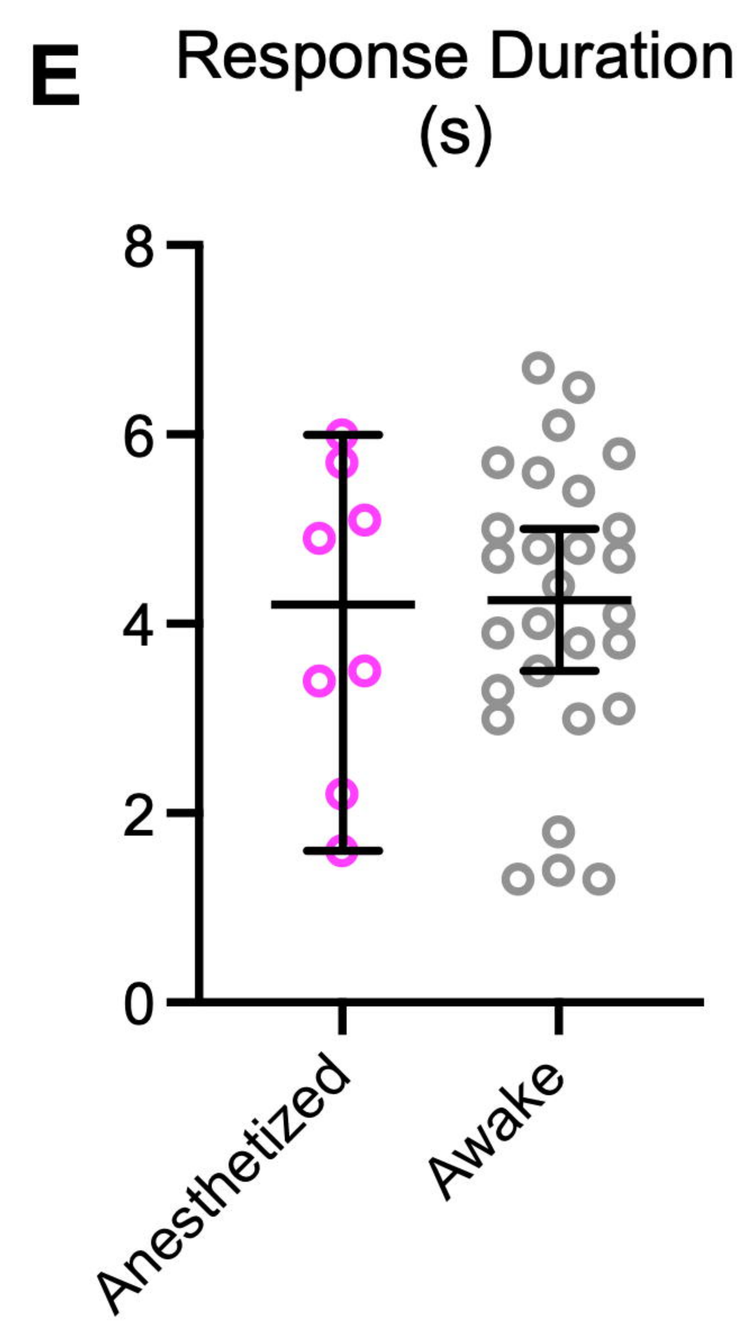
E
Response Duration (s)
8
6
4
2
0
Anesthetized
Awake

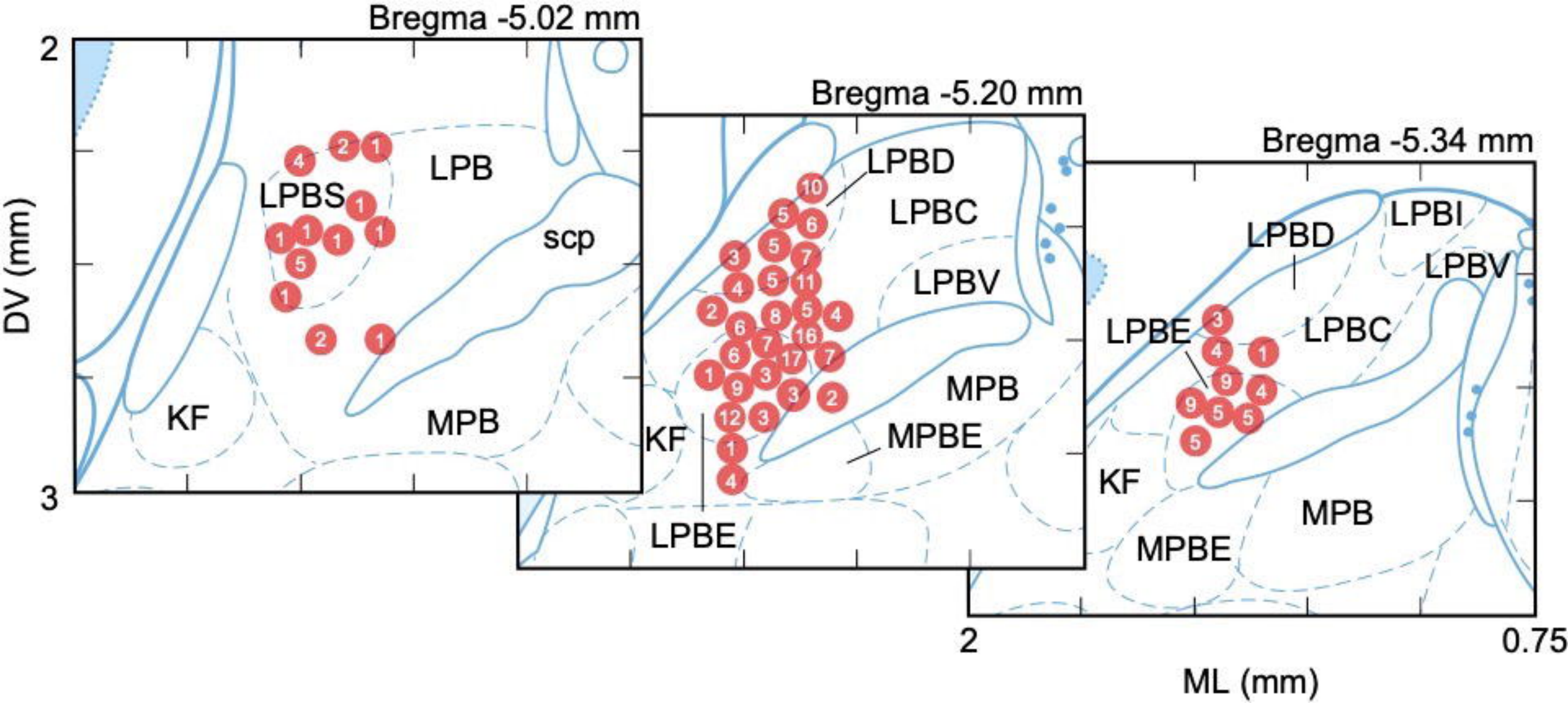
Bregma -5.02 mm
Bregma -5.20 mm
Bregma -5.34 mm
DV (mm)
2
3
LPB
LPBS
scp
KF
MPB
LPBD
LPBC
LPBV
MPBE
LPBE
LPBI
2
0.75
ML (mm)

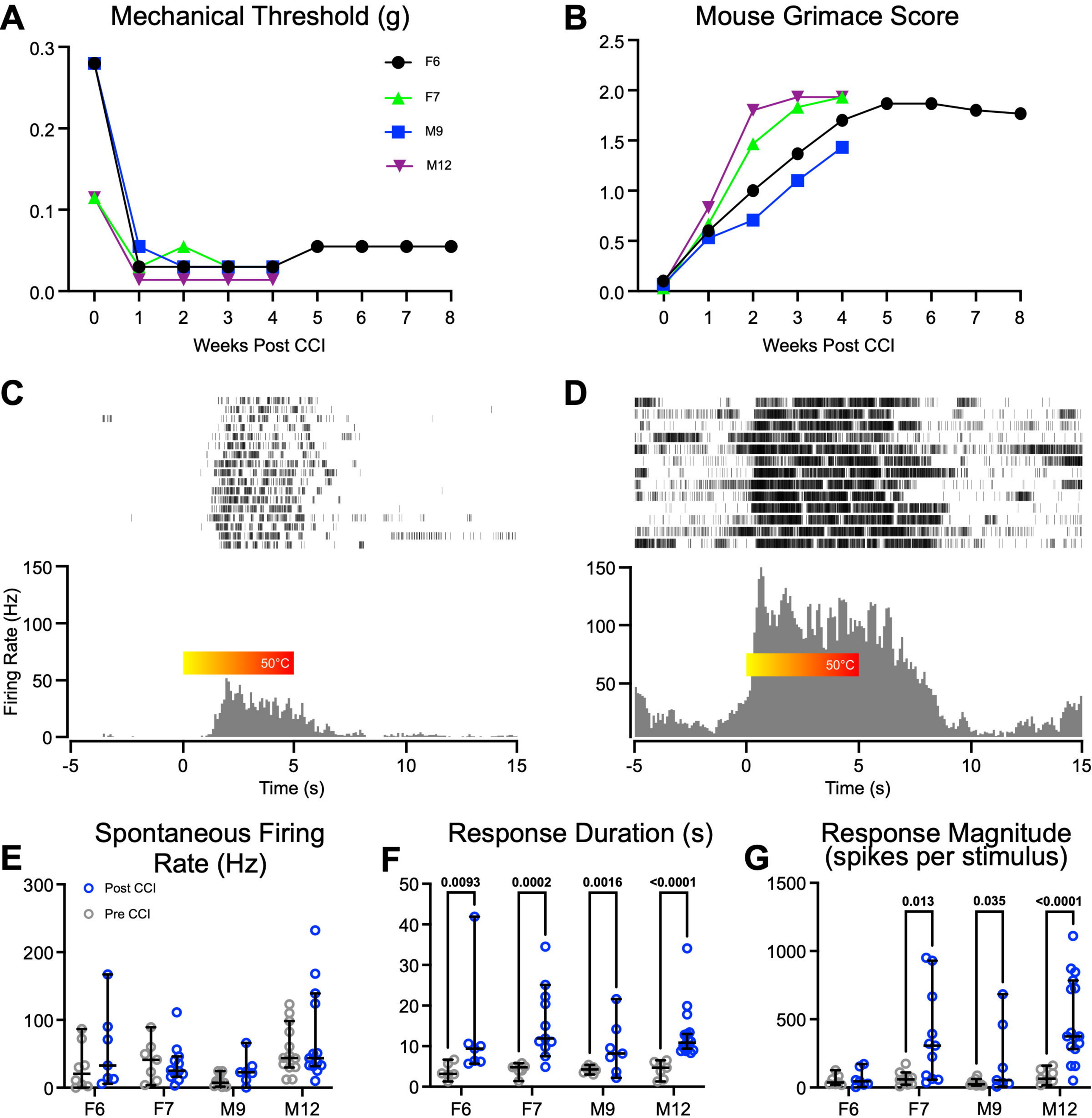
A
Mechanical Threshold (g)
0.3
0.2
0.1
0.0
F6
F7
M9
M12
0 1 2 3 4 5 6 7 8
Weeks Post CCI
B
Mouse Grimace Score
2.5
2.0
1.5
1.0
0.5
0.0
0 1 2 3 4 5 6 7 8
Weeks Post CCI
C
D
Firing Rate (Hz)
150
100
50
0
50°C
-5 0 5 10 15
Time (s)
E
Spontaneous Firing Rate (Hz)
Post CCI
Pre CCI
300
200
100
0
F6 F7 M9 M12
F
Response Duration (s)
0.0093
0.0002
0.0016
<0.0001
50
40
30
20
10
0
F6 F7 M9 M12
G
Response Magnitude (spikes per stimulus)
0.013
0.035
<0.0001
1500
1000
500
0
F6 F7 M9 M12

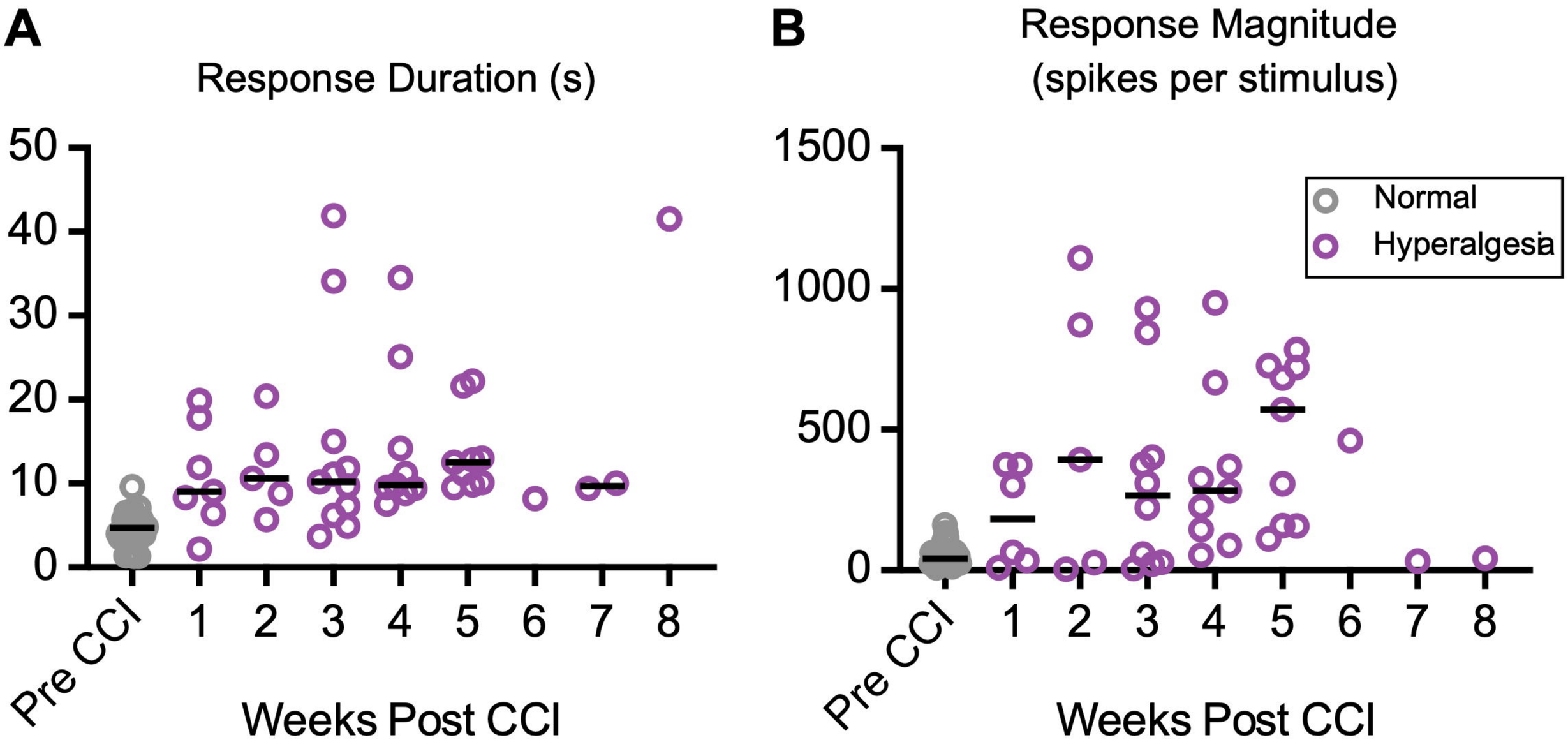
A
Response Duration (s)
50
40
30
20
10
0
Pre CCI
1
2
3
4
5
6
7
8
Weeks Post CCI
B
Response Magnitude
(spikes per stimulus)
1500
1000
500
0
Normal
Hyperalgesia
Pre CCI
1
2
3
4
5
6
7
8
Weeks Post CCI

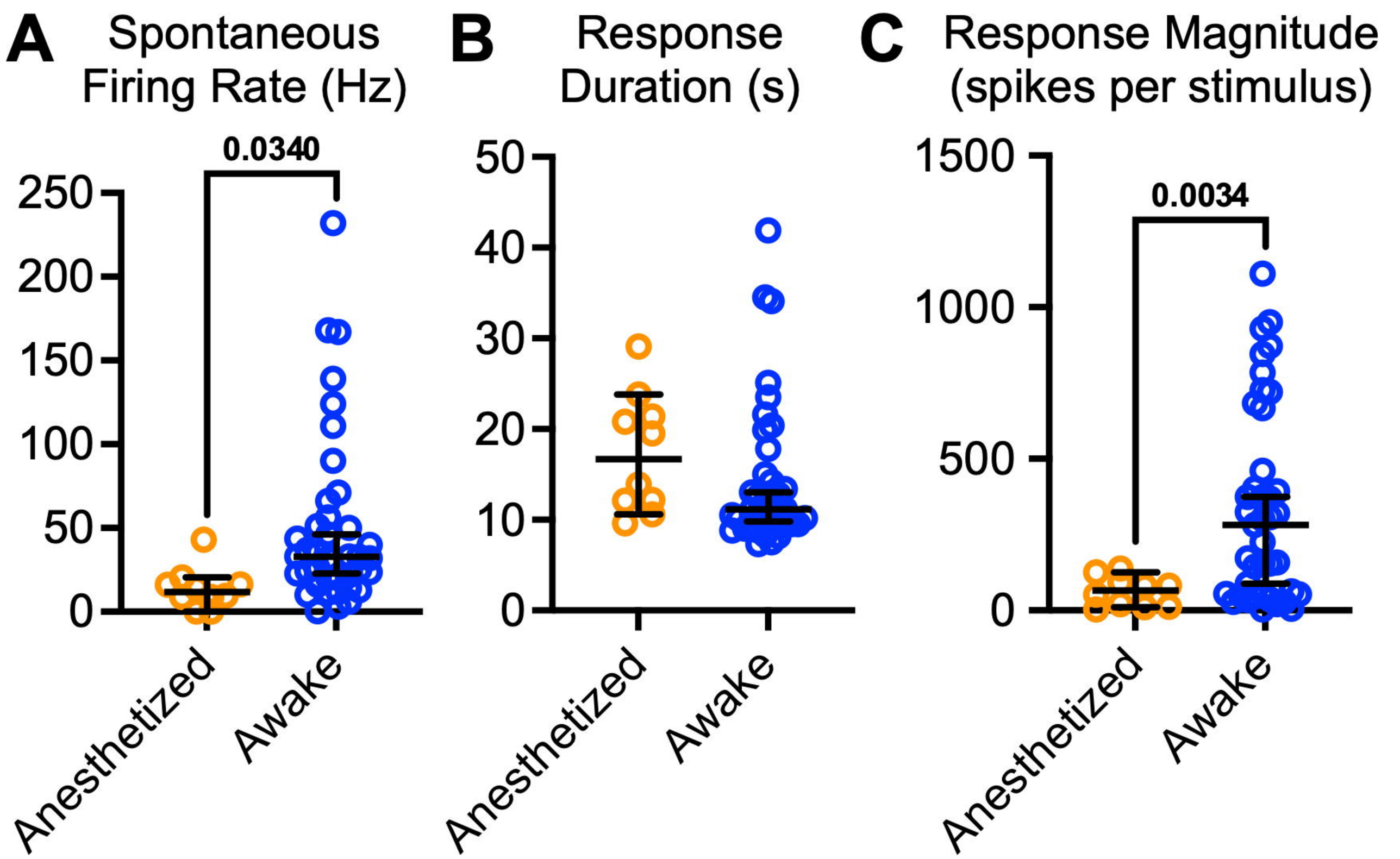
A
Spontaneous Firing Rate (Hz)
0.0340
250
200
150
100
50
0
Anesthetized
Awake
B
Response Duration (s)
50
40
30
20
10
0
Anesthetized
Awake
C
Response Magnitude (spikes per stimulus)
1500
1000
500
0
0.0034
Anesthetized
Awake

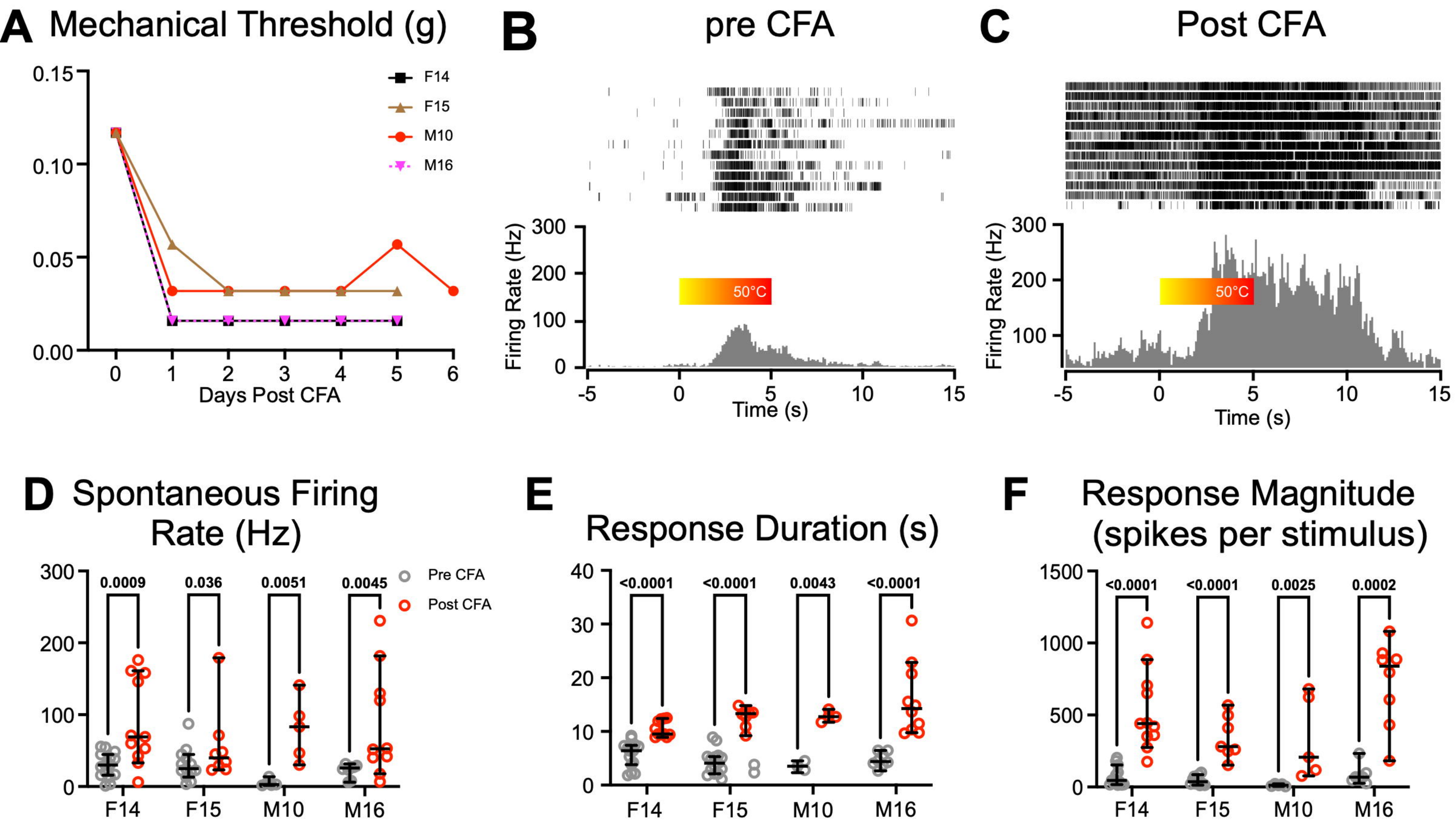
A
Mechanical Threshold (g)
0.15
0.10
0.05
0.00
F14
F15
M10
M16
0
1
2
3
4
5
6
Days Post CFA
B
pre CFA
Firing Rate (Hz)
300
200
100
0
50°C
-5
0
5
10
15
Time (s)
C
Post CFA
Firing Rate (Hz)
300
200
100
50°C
-5
0
5
10
15
Time (s)
D
Spontaneous Firing Rate (Hz)
300
200
100
0
0.0009
0.036
0.0051
0.0045
Pre CFA
Post CFA
F14
F15
M10
M16
E
Response Duration (s)
40
30
20
10
0
<0.0001
<0.0001
0.0043
<0.0001
F14
F15
M10
M16
F
Response Magnitude (spikes per stimulus)
1500
1000
500
0
<0.0001
<0.0001
0.0025
0.0002
F14
F15
M10
M16

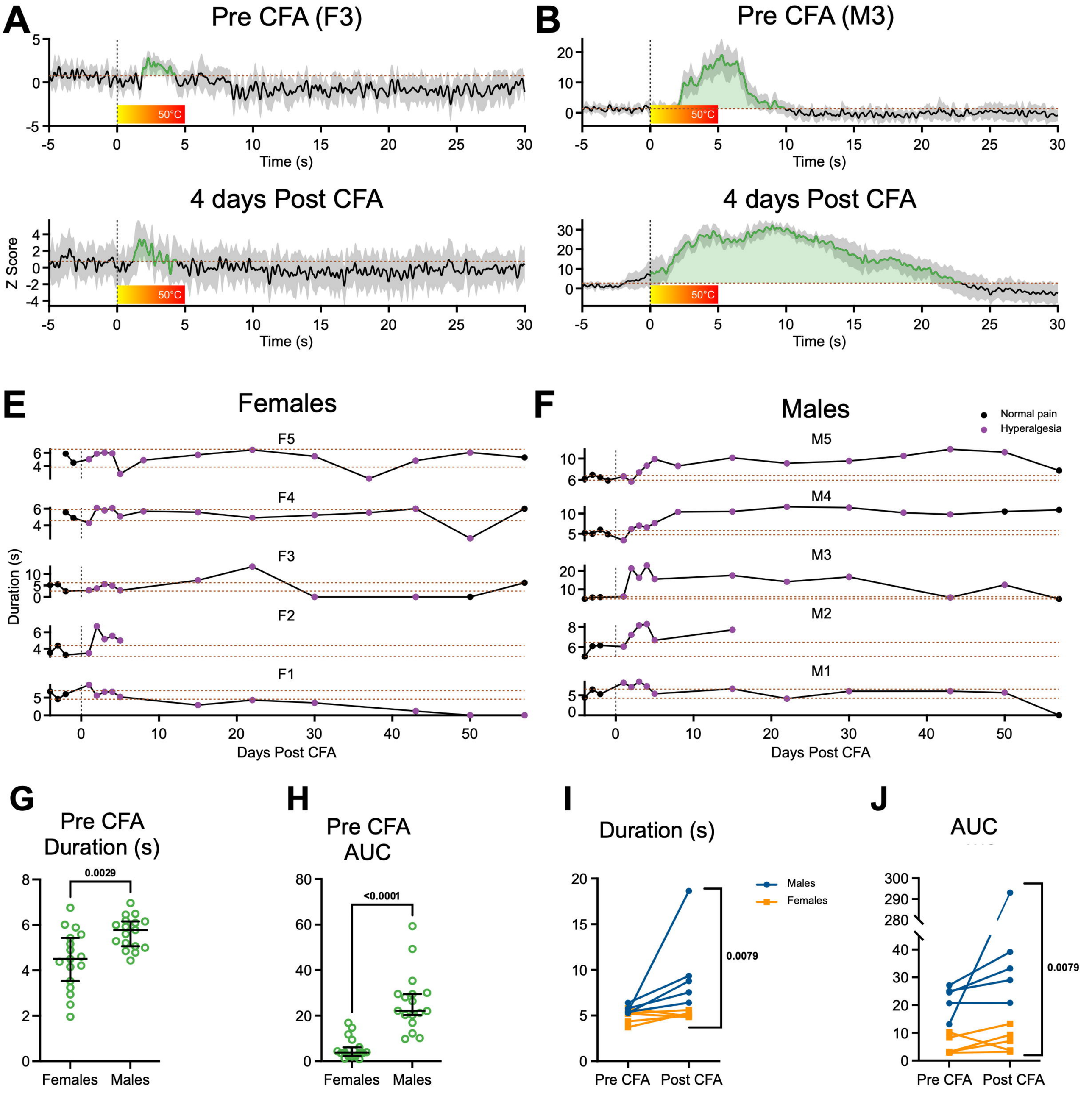
A
Pre CFA (F3)
B
Pre CFA (M3)
4 days Post CFA
4 days Post CFA
Z Score
50°C
Time (s)
E
Females
F
Males
Normal pain
Hyperalgesia
F5
F4
F3
F2
F1
M5
M4
M3
M2
M1
Duration (s)
Days Post CFA
G
Pre CFA
Duration (s)
0.0029
Females
Males
H
Pre CFA
AUC
<0.0001
I
Duration (s)
Males
Females
0.0079
Pre CFA
Post CFA
J
AUC
0.0079

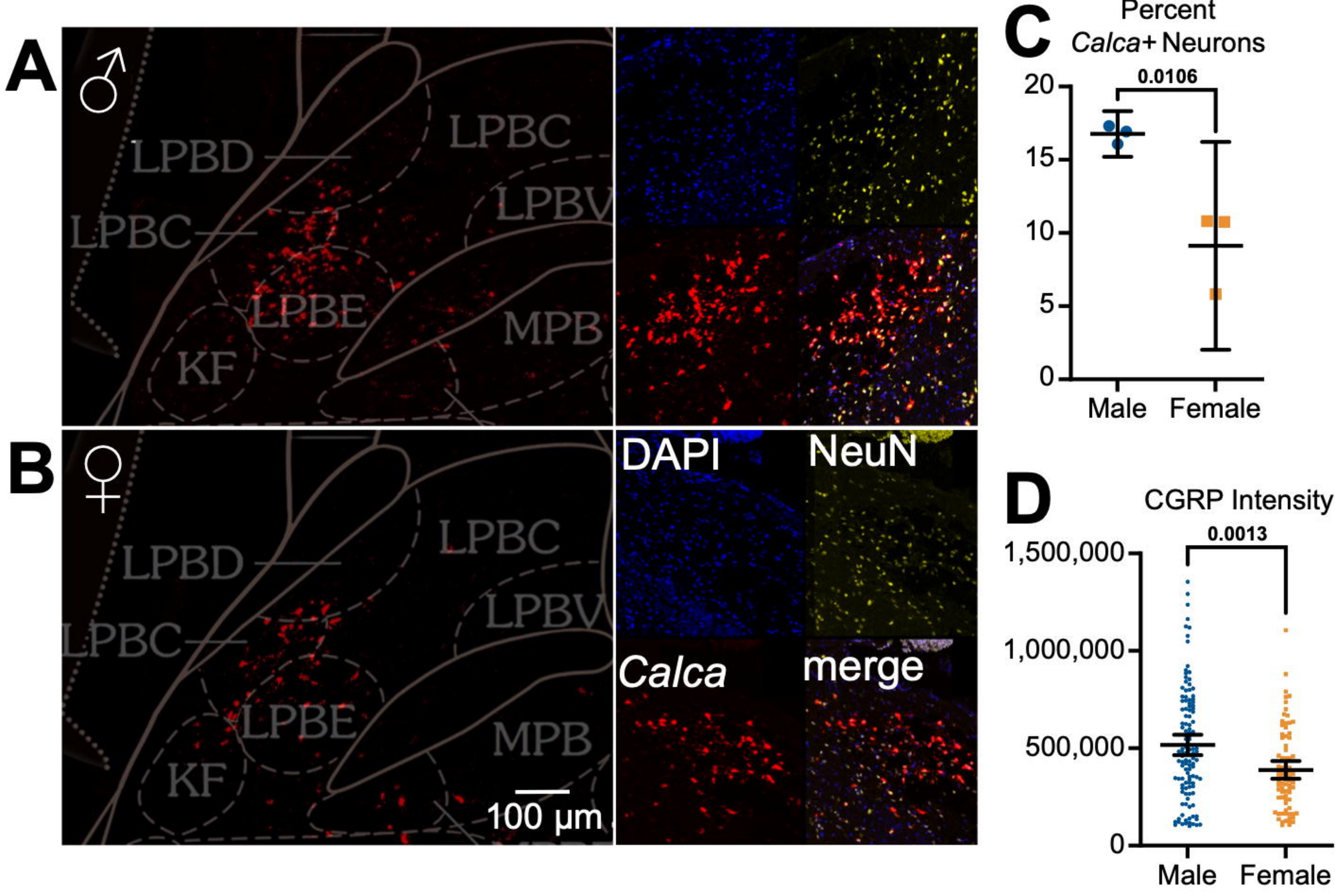
A
B
LPBD
LPBC
LPBV
LPBE
MPB
KF
100 µm
DAPI
NeuN
Calca
merge
C
Percent
Calca+ Neurons
0.0106
20
15
10
5
0
Male
Female
D
CGRP Intensity
0.0013
1,500,000
1,000,000
500,000
0
Male
Female

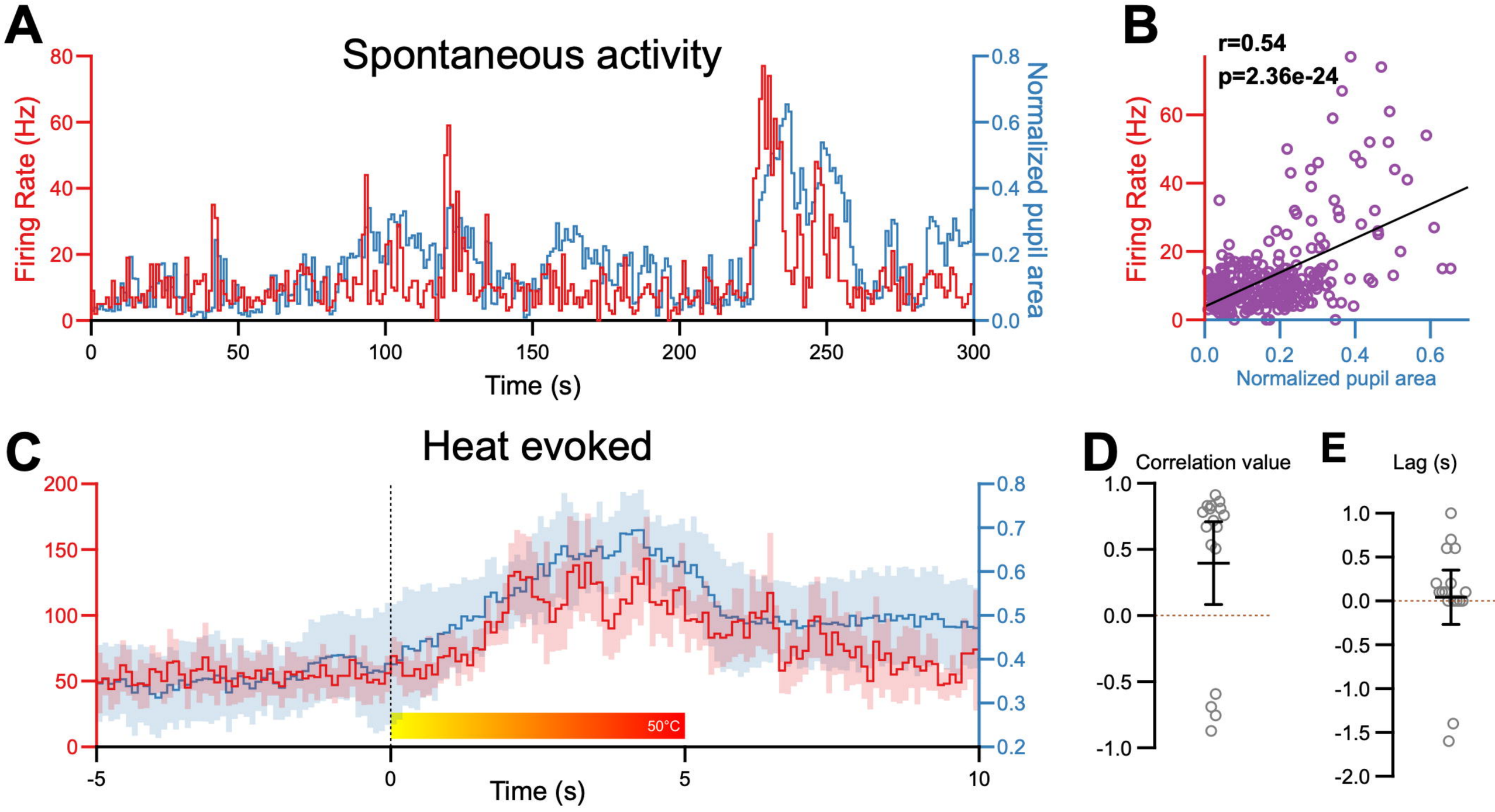
A
Spontaneous activity
Firing Rate (Hz)
Normalized pupil area
Time (s)
B
r=0.54
p=2.36e-24
Firing Rate (Hz)
Normalized pupil area
C
Heat evoked
50°C
Time (s)
D
Correlation value
E
Lag (s)

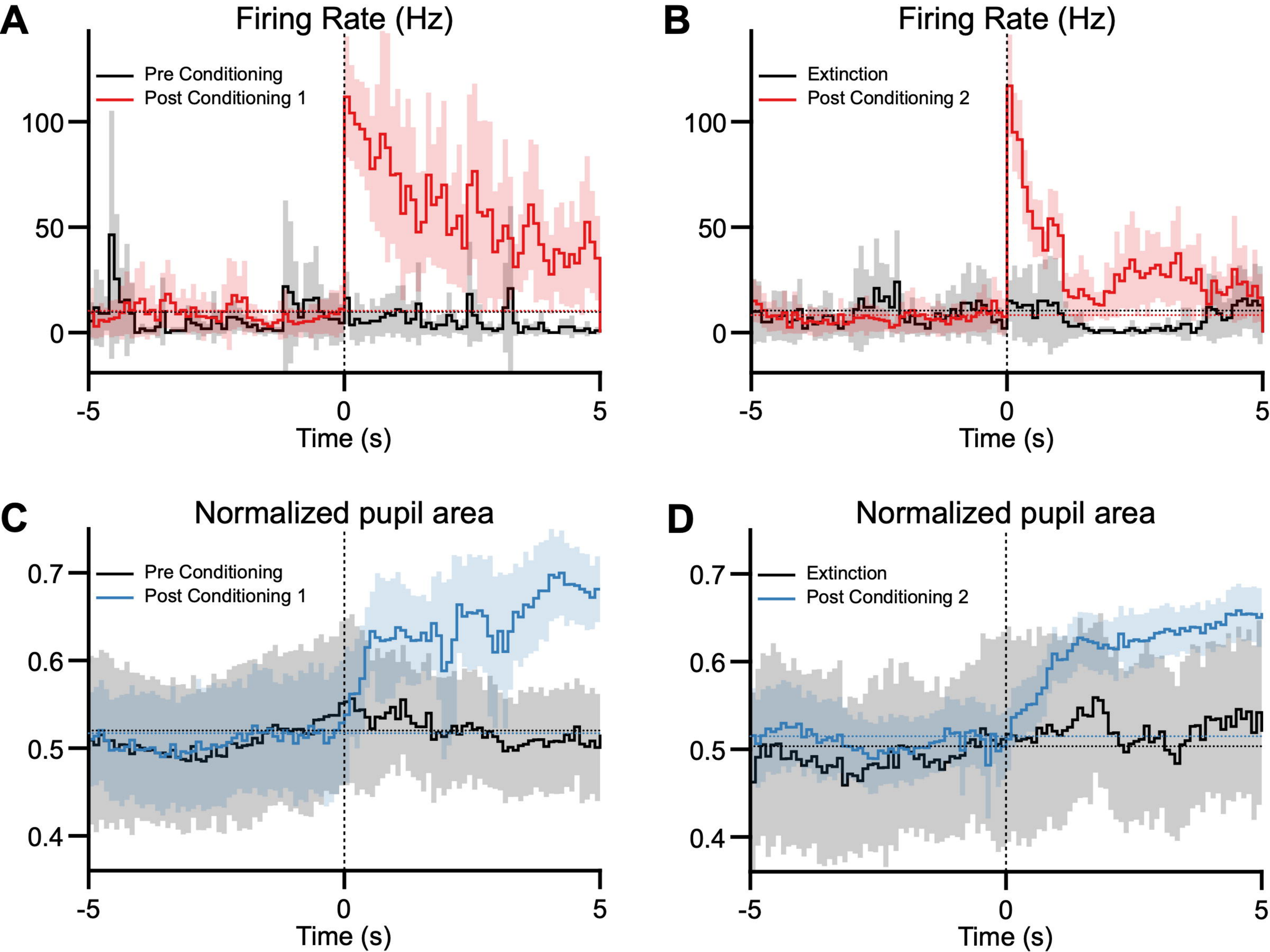
A
Firing Rate (Hz)
Pre Conditioning
Post Conditioning 1
100
50
0
-5
0
5
Time (s)
B
Firing Rate (Hz)
Extinction
Post Conditioning 2
100
50
0
-5
0
5
Time (s)
C
Normalized pupil area
Pre Conditioning
Post Conditioning 1
0.7
0.6
0.5
0.4
-5
0
5
Time (s)
D
Normalized pupil area
Extinction
Post Conditioning 2
0.7
0.6
0.5
0.4
-5
0
5
Time (s)